Scaling Hydraulic Conductivity by Applying Laplacian with Skin to Fractures Network

Harol Alexander Cetre Orejuela

Universidad EAFIT

Department of Earth Science

Medellín, Colombia

2021

Scaling Hydraulic Conductivity by Applying Laplacian with Skin to Fractures Network

Harol Alexander Cetre Orejuela

Thesis presented as a requirement to apply for the title of:

Magister en Ciencias de la Tierra

Director (a):

(Ph.D) Marcela Jaramillo

Codirector (a):

(Ph.D) Oscar David Álvarez Villa

Research track: Groundwater Modeling in Fractured Medium

Research Group: Ciencias del Mar

Universidad EAFIT

Department of Earth Science

Medellín, Colombia

2021

Escojamos lo que escojamos, siempre tenemos que preguntarnos cuáles serán las consecuencias.

James Lovelock

Acknowledgements

To GOD for the life and the option to decide. To my parents Doris y Thelmo for their love and tireless dedication. Thank you for such a valuable heritage; you are my greatest pride.

I want to express my sincere gratitude to my advisors, Marcela Jaramillo and Oscar Álvarez, for their support, patience, and valuable contribution of knowledge in my academic growth; without them this work would not have been possible.

To Yulitsa for her support and always being with me in this incredible experience. To my fellow masters for the contribution of knowledge and experiences, especially Aura for her invaluable support.

I am grateful to the company Pi Épsilon S.A.S for supporting my master's studies and giving me the confidence and space necessary to study and work; thank you for this valuable opportunity.

Table of Contents

1 Introduction

The Discrete Fracture Network (DFN) method stands out for detailed modeling of groundwater flow through fractures because each element of the fractures network can be analyzed independently (Ren et al., 2017). Although the DFN method provides greater detail when simulating flow through fractures than other methodologies, it requires describing all the network elements' geometry and hydraulic properties. This detailed description of the fracture network geometry could make the DFN method impractical for regional groundwater flow modeling (Teutsch, 1993) due to the high computational requirements (Cook et al., 2003).

On the other hand, modeling groundwater flow in a fractured medium using distributed strategies has been limited, primarily because of the scale problems from representing fracture networks by regular blocks with equivalent hydraulic parameters. This methodology is commonly known as the continuous approach. Some of the most recurrent scale problems of modeling groundwater flow in fractured medium with a continuous approach are:

- The implementation of distributed groundwater flow models requires hydraulic parameters for each of the discretization elements. Nevertheless, the size of a model block is usually several orders of magnitude greater than the hydraulic conductivity measurement scale (Tran, 1995). This disparity between the observational and modeling scales could have undesirable consequences when implementing regional models using hydraulic tests performed locally on individual fractures.
- The opening, orientation, density, and persistence are geometric properties of fractures commonly used in estimating the hydraulic parameters of fractured rocks. Such geometric properties can only be observed in rocks exposed on the land surface, in wells of a determined size, in the walls of underground excavations, and on hydraulic tests with limited spatial scope (Jing & Stephansson, 2007). Traditional sampling strategies of rock hydraulic conductivity do not provide a comprehensive description of the entire fracture network, especially in studies at the regional scale.

The DFN method is usually used in the Equivalent Porous Media (EPM) method to represent fractured medium as a continuous medium (Neuman, 2005; Ouenes & Hartley, 2000). In this

context, the EPM method assumes that it is possible to estimate the equivalent hydraulic conductivity of a DFN within a volume of rock if an estimate of the representative elementary volume (REV) is available (Bear, 1972). Therefore, if the DFN is representative at the measurement scale, an upscaling procedure allows obtaining the fractured rock's hydraulic parameterization.

Hydraulic conductivity scaling is a procedure for transforming information between scales. This transformation allows us to represent the fine-scale variability of the hydraulic conductivity at the block scale (Botros et al., 2006; Gupta et al., 1986; Indelman & Dagan, 1993). By definition, the fine-scale or sampling scale refers to the spatial extent of a data set (Blöschl & Sivapalan, 1995). The block scale or numerical scale refers to the size of numerical models' cells (Wen & Gómez-Hernandez, 1996).

Considering that scaling allows us to transform data sources at different scales and combine them for creating a consistent modeling framework, this research presents a review of the main methods for scaling hydraulic conductivity. By weighing the pros and cons of the currently existing scaling methodologies, the following research questions emerge:

(i) Can the hydraulic conductivity of a fractured medium be scaled by applying Laplacian with the skin to a network of fractures?

(ii) In what measure does the upscaling procedure reduce the computational burden of the upscaled models?

To answer the previous questions, the following assumptions are adopted: (i) it is possible to calculate the hydraulic conductivity tensor on a thick scale using the Laplacian with skin technique, (ii) it is possible to generate a fracture network domain, discretize the area and determine the hydraulic conductivity within each subdomain, (iii) considering the full tensor of hydraulic conductivities when solving the groundwater flow equations helps to circumvent numerical inconsistencies of the upscaling procedure, and (iv) upscaling the hydraulic conductivity helps us to produce more efficient surrogate models applicable at the regional scale.

This research had two main objectives. The first was to use the Laplacian with Skin technique to scale the fracture network's hydraulic conductivity in order to represent, in the block scale, the average dynamics of the flow and hydraulic heads observed in the fine-scale. The second was to reduce the times and computational load of the evaluation of fractured medium models.

This document contains two main chapters (2 and 3), each written following an academic paper's structure. Chapter 2 is entitled *Scaling of Hydraulic Conductivity in Fractured Medium for*

Continuous Models: A Review, which contains the description of the scale and hydrogeological modeling problems that motivated the research, and an extensive bibliographic review of the leading hydraulic conductivity scaling techniques. From this review, the Laplacian-with-skin method was selected as a tool for scaling fractures rock hydraulic conductivity. Chapter 3 presents the article *Calculation of Hydraulic Conductivity Tensor in 2D Applying Laplacian with Skin to Fractures Network*, which contains the description of a fracture network scaling tool implemented in Python 3, based on the operation of the method of generation of DFN fractures and the operation of the Laplacian technique with skin. This chapter also shows the results of an application case with which the scaling tool was tested.

Chapter 4 presents the thesis's general conclusions, elaborated from the results found in chapters 2 and 3. It should be noted that for each article, the conclusions are presented within the chapters. Finally, chapter 5 brings together the bibliographic references of chapters 1, 2, 3, and 4.

2 Scaling of Hydraulic Conductivity in Fractured Medium for Continuous Models: A Review

Harol Alexander Cetre-Orejuela, Marcela Jaramillo, Oscar David Álvarez-Villa

Abstract: Hydraulic conductivity exhibits a high spatial variability due to the heterogeneity and discontinuity between a geologic environment's constituent materials. Representing such variability is a problem when implementing groundwater flow models, especially in fractured rock media. In those cases, the hydraulic tests performed in the fractures constitute measurements at the fine or local scale. Nevertheless, groundwater flow models are usually built to respond to problems that involve the regional scale, with a discretization of several orders of magnitude greater than the fine-scale. Despite the recent advances in supercomputing, modeling groundwater flow in fractured rock using the DFN method at the regional scale is still considered problematic. The impossibility of hydraulically characterizing the entire fracture network, and the high computational cost of detailed regional models at the discrete fracture level, make the use of models with a continuous focus in regional modeling more practical. This article presents a review of the most widely used hydraulic conductivity scaling techniques, searching to identify a method that allows us to improve fractured medium representation as a continuum based on equivalent hydraulic parameters.

2.1 Introduction

Groundwater flow models are simplified representations of the complex fluxes occurring in the geological medium at different time and space scales (Anderson et al., 2015; Bear & Cheng, 2010; H. F. Wang & Anderson, 1982). In this regard, different modeling approaches exist for implementing groundwater flow models depending on the type of geological medium on which the flow occurs. In the case of modeling groundwater flow in fractured rocks, the most popular modeling frameworks are the Discrete Fractures Network (DFN) and the Equivalent Porous Media (EPM) models (Molinero et al., 2002).

The DFN method poses that each fracture network element is independent of the other network members (Ren et al., 2017). Consequently, the flow circulating through each fracture can be modeled individually (Berkowitz, 2002).

The first applications of DFN models in real problems were restricted to small spatial scales due to the computers' low available capacity at that time (Cacas et al., 1990). In general, the primary information required for applying the deterministic DFN method is the location, the geometry, and the hydraulic properties of each fracture (Scanlon et al., 2003). Alternatively, the implementation of stochastic DFN models requires a probability distribution of the previously mentioned parameters. The impossibility of densely sampling the DFN parameters (Renard & de Marsily, 1996) and the numerical solvers' immense computational burden (Lei et al., 2017; H. Zhou, 2010) are the main limitations for applying the DFN method at the regional-scale geologic domains. Despite such drawbacks, the DFN method has been applied to regional-scale analysis for determining the potential migration paths of solute plumes in fractured rocks (Cvetkovic et al., 2004; Dershowitz et al., 1991; Fadakar Alghalandis, 2017; Huang et al., 2016). The method has also been used for estimating the equivalent hydraulic conductivity of a rock volume to represent it as a continuum (Ghasemizadeh et al., 2015; Hadgu et al., 2017; Long et al., 1982; Neuman, 2005; Ouenes & Hartley, 2000).

When modeling fractured rock as a continuum, the rock matrix and fractures system are encompassed into an EPM with equivalent hydraulic parameters. With this conceptualization, the fracture network becomes a part of the newly formed equivalent media's primary porosity, and the variability inside the scaling volume is neglected (Wanfang et al., 1997). Once the configuration of the EPM is available, it is possible to use the continuity and the momentum conservation equations for creating constitutive models of groundwater flow within the equivalent medium (Assteerawatt, 2008).

The EPM approach has been used to construct regional groundwater models in fractured media (Ghasemizadeh et al., 2015; Scanlon et al., 2003). Its usefulness extends from the simulation of changes in the components of the water balance and optimization of groundwater development scenarios to its use as tools to predict future dynamics in the face of human activities impacts (Y. Zhou & Li, 2011). In terms of disadvantages, some authors highlight two aspects of the EPM approach: the non-reproduction of behaviors on a fine-scale (Cacas et al., 1990) and the inefficiency for simulating regional flows in highly karstified aquifers using a single continuum approach (Teutsch, 1993). Notwithstanding the above, previous research has shown that the EPM method can produce good regional fractured medium models. An example is the International Stripa Project (Dershowitz et al., 1991; Herbert et al., 1991). There, continuous models

implemented using the EPM method offered performance comparable to those created via the DFN framework. Likewise, Ando et al. (2003) concluded that a high-resolution stochastic continuous flow model built for an aquifer in the region of Fanay-Augéres (France) worked as well as the DFN-based models implemented by (Cacas et al., 1990). Finally, Neuman (2005) highlights that, even though the DFN models incorporate much more detail for modeling groundwater flow in fractured media, such models typically do not outperform continuous models.

One of the biggest problems of modeling flow in a fractured medium on a regional scale is the lack of representativity of the hydraulic conductivity estimates from hydraulic tests such as Lugeon, slug tests, single-well flowmeter tests, and fiber optic tests (Klepikova et al., 2011; Lavenue & Marsily, 2001; Maréchal et al., 2007; Suescún, 2016; T. Wang et al., 2015; Wyllie & Mah, 2007). Such estimates typically represent areas that vary from centimeters to a few meters (King, 1989; Wen & Gómez-Hernandez, 1996). Furthermore, their use in block models requires adequate treatment since the hydraulic parameters are the source of the most significant uncertainty in the modeling (Hassan et al., 2008; Siade et al., 2017). An equivalent hydraulic conductivity tensor can represent the fine-scale variability of the hydraulic conductivity in a fractured media (Gómez-Hernández, 1991). Applying this premise, a distributed tensorial strategy could be useful to describe the small-scale variability within the EPM blocks in a regional model. Gómez-Hernández (1991) showed that these tensors provide a more accurate representation of the small-scale flow dynamics than a simple average or even more complex estimators.

Obtaining reliable hydraulic conductivity estimates for implementing regional groundwater models from local samplings is still an open problem in hydrogeology. Given its dual nature, solving the problem mentioned above is even more difficult for fractured media. With this in mind, throughout this article, we present a bibliographic review of the more relevant scaling techniques of hydraulic conductivity, with a focus on methods suitable for applications in fractured media.

2.2 Spatial variability of hydraulic conductivity

Hydraulic conductivity is highly variable in space due to different factors: the geological settings, the lithological variation, and the media discontinuities (Maréchal et al., 2007; Martinez-Landa & Carrera, 2006). Previous studies have demonstrated that this variability occurs even for the same type of materials and depends on measurement scale (Schulze- Makuch et al., 1999). Estimates of hydraulic conductivity from laboratory tests could differ in many orders of magnitudes regarding measurements from field experiments. Furthermore, considerable differences in hydraulic conductivity estimates are frequent for samples of soil and rock representing the same analysis scale and are extracted from the same geological materials (Piña et al., 2019).

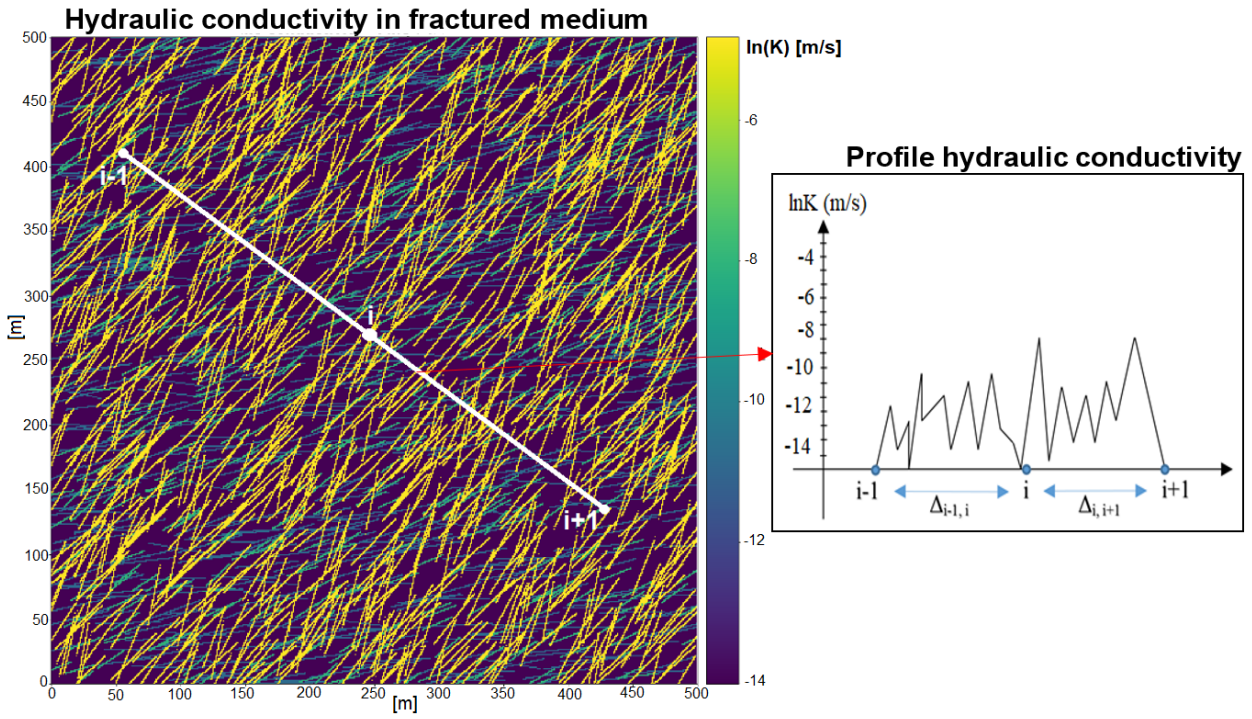

Figure 1. Example of spatial variability of hydraulic conductivity in a two-dimensional heterogeneous medium. The white line [i-1, i+1] represents a transect with conductivity changes from one point to another. The profile (plot in the right) represents the hydraulic conductivity values schematically for each cell in the transect as a function of the distance. The color palette indicates the values of the hydraulic conductivity—own elaboration.

Figure 1 presents the variability of the hydraulic conductivity in a fractured medium due to the contrast between the rocky matrix's hydraulic properties and the fractures. The white line represents a trajectory along which we want to calculate the flow. We discretize this system in several sub-components, for example [i-1, i] and [i, i+1]. We want to calculate the respective flow using the hydraulic gradient for each sub-component and a representative value of the hydraulic conductivity. The previous approach generates the following question: How do we calculate a convenient value of each component's hydraulic conductivity to obtain accurate flow estimations along the whole transect? We can answer this question by calculating an average value of hydraulic conductivity that preserves the flows for a given hydraulic head value, for example, the harmonic mean. Nonetheless, the estimation's complexity increases for two and three-dimensional domains because the harmonic mean expression used to estimate the conductivity is limited to some geometric configurations and some scales (Freeze, R.A., Cherry, 1979).

When representing a fractures network as a continuous medium using the EPM method, the spatial variability of the hydraulic conductivity can be expressed by an equivalent parameter if the Representative Elementary Volume (REV) assumption is valid (Long et al., 1982). The REV is the minimum volume of fractured rock for which the hydraulic conductivity does not vary substantially

with the increase in the volume analyzed (Bear, 1972; Kulatilake et al., 2000; Ren et al., 2017). The fractured system must be homogeneous in terms of the statistical distribution of the geometric variables of fractures-density, orientation, and size (Londoño Aguirre, 2015).

Now, let us assume that the concept of REV is applicable at the modeling scale. In that case, we can use the equations of continuity and conservation of momentum (generalized Darcy's law) to solve the generalized groundwater flow equation (Bear et al., 1993; Berkowitz et al., 1988; Durlofsky, 1991), as follows:

$$\nabla(K.\nabla h) = S_s \frac{\partial h}{\partial t} + Q \quad \text{(Eq. 2.1)}$$

where, ∇ is the divergence operator $\left(\frac{\partial}{\partial x} + \frac{\partial}{\partial y} + \frac{\partial}{\partial z}\right)$, ∇h (L) is the hydraulic gradient for the three orthogonal directions $\left(\frac{\partial h}{\partial x}, \frac{\partial h}{\partial y}, \frac{\partial h}{\partial z}\right)$, S_s (dimensionless) is the specific storage coefficient, Q (L^3/T) represents the external actions of the system, and K (L/T) is the hydraulic conductivity tensor, defined as:

$$K = \begin{bmatrix} k_{xx} & k_{xy} & k_{xz} \\ k_{yx} & k_{yy} & k_{yz} \\ k_{zx} & k_{zy} & k_{zz} \end{bmatrix} \quad \text{(Eq. 2.2)}$$

where, k_{xx}, k_{yy} and k_{zz} (L/T) are the main components in x, y, and z directions, and the remaining terms represent the conjugate values of hydraulic conductivity tensor. The existence of the REV is conditioned to the density of fractures and the fracture systems' connectivity in the rock, which means that it is not always possible to estimate the REV (Cacas et al., 1990). Additionally, some media show low fracture density, causing them to be represented only as a continuum on some scales (Kulatilake et al., 2000).

2.3 Hydraulic conductivity upscaling

Constructing regional-scale groundwater flow models using hydraulic conductivity data sampled at a small scale raises the problem of estimating new values representative for the scale change. This procedure is widely known as upscaling (Sanchez-Vila et al., 2006). In this section, we describe some of the most used hydraulic conductivity scaling techniques. We present the scaling techniques based on the medium to which they have been applied and the type of hydraulic conductivity, as follows: we group the techniques that scale the hydraulic conductivity in a porous medium and separate them from the techniques that scale the hydraulic conductivity in a fractured medium. We differentiate the techniques that calculate a single hydraulic conductivity value from

those that calculate a tensor quantity for each group. We highlight the applicability of fractured rocks' latest methods for upscaling hydraulic conductivity in regional modeling applications.

2.3.1 Methods for scaling hydraulic conductivity to single value – porous medium

- **Sample and power average**

The use of simple averages or power averages for scaling hydraulic conductivity in one or two-dimensional blocks depends on its probability distribution function and spatial correlation degree (Renard & de Marsily, 1996). The one-dimensional scaling problem is relatively simple because the block hydraulic conductivity can be estimated directly using the harmonic mean. For the two-dimensional case, Matheron (1967) proved that the best estimator for the block hydraulic conductivity is the geometric mean if the probability distribution at the sampling scale is log-normal. Other authors (Bouwer, 1969; Durlofsky, 1992; Warren & Price, 1961) explored different upscaling estimators (arithmetic, geometric and harmonic averages) for different mediums on which the hydraulic conductivities showed low or zero spatial correlation. Their results proved that none of these simple averages could be used as a generalized estimator of the upscaled hydraulic conductivity at the block scale. Journel et al. (1986), based on Cardwell & Parsons' (1945) work, proposed that the effective block hydraulic conductivity can be estimated using an average of order P. Equivalent hydraulic conductivities estimated via the average of order P are bounded by the arithmetic and harmonic mean. Mathematical expressions for calculating the simple, harmonic, geometric, and power averages, respectively, are the following:

$$K_v = \frac{1}{n}\sum ki \qquad \text{(Eq. 2.3)}$$

$$K_v = \frac{n}{\sum_{i=1}^{n}\frac{1}{k_i}} \qquad \text{(Eq. 2.4)}$$

$$K_v = \sqrt[n]{k_1 k_2 k_3 \dots k_n} \qquad \text{(Eq. 2.5)}$$

$$K_V = \frac{1}{V}\left(\int_V K_w^p(u)du\right)^{1/p} \qquad \text{(Eq. 2.6)}$$

where K_v (L/T) is the hydraulic conductivity value of the block, k_i (L/T) hydraulic conductivity in fine scale, V (L^3) volume of the block, and p (dimensionless) the power. In cases on which $p = -1$, equation 2.6 becomes the harmonic mean estimator. Similarly, if $p = 1$ in equation 2.6 represents the simple average.

- **Renormalization**

Renormalization is a mathematical methodology to study phenomena with various spatial scales (Shah & Ottino, 1986). In the hydraulic conductivity case, renormalization calculates a representative value for reproducing approximately the fine-scale flow at the block scale, given a hydraulic gradient (King, 1989; Loc'H, 1987). The method estimates the effective hydraulic conductivity for a mesh of conductivities by scaling recursively. In a first scaling step, hydraulic conductivity blocks are generated by applying harmonic averages in the x and y directions on the fine scale values. Subsequently, the scaling of the blocks continues until a single hydraulic conductivity value is obtained in both directions for the entire mesh. The effective hydraulic conductivity is calculated by applying the geometric mean to the harmonic averages of the block (Renard & de Marsily, 1996):

$$K_b^{xx} = \sqrt{c_{max}^{xx} c_{min}^{xx}} \quad \text{(Eq. 2.7)}$$

where, c_{max}^{xx} and c_{min}^{xx} (L/T) are the extreme values that correspond to the harmonic mean from grouping in a series of hydraulic conductivity.

- **Perturbation and Self-Consistent Approach**

The perturbation method calculates the effective hydraulic conductivity for a heterogeneous medium by using the moments of the hydraulic conductivity distribution function (De Wit, 1995), as follows:

$$K_{eff}^{jm} = K_G \left[\left(1 + \frac{\sigma^2}{2} \right) \delta_{jm} - \sigma^2 \alpha_{jm} \right] \quad \text{(Eq. 2.8)}$$

where, K_{eff}^{jm} (L/T) is the effective hydraulic conductivity, σ^2 is the variance, K_G (L/T) is the geometric mean of the log-permeability, δ_{jm} (dimensionless) is the Kronecker delta, and α_{jm} is a tensor that depends only on space dimensions and anisotropy ratios. Consequently, the effective hydraulic conductivity is defined by the sum of an average and a spatially dependent function (Stepanyants & Teodorovich, 2003). Indelman (1996) applied the perturbation method to calculate an effective parameter in random means of stationary conductivity and related the average velocities with the average flows. Noetinger (1994) estimated effective hydraulic conductivities via the partial series resumption technique on an infinite aquifer. This application aimed to develop an upscaling method that converges faster than the power series technique used by King (1987) for log-normally distributed hydraulic conductivity.

The approximation of solutions through small perturbations of the continuity equation assumes that the hydraulic conductivity's standard deviation is small compared to its mean. This assumption

limits the method's applicability to formations with high variability (Dagan, 1979, 1981). The self-consistent approach constitutes an extension of the perturbation method on which the limits method (Beran & Pytte, 1968) conditions the perturbations. This modification allows a more reliable application of the method in heterogeneous formations. The limit method operates in two steps. First, it determines the upper and lower limits of the effective conductivity. Second, it uses a predefined frequency distribution function to determine the mean conductivity of the heterogeneous medium as:

$$k_{eff} = \frac{1}{n}\left[\int_{k_{min}}^{k_{max}} \frac{p(k)}{k+(n-1)\mathrm{k}^*} dk\right]^{-1} \quad \text{(Eq. 2.9)}$$

where, k_{eff} (L/T) is the effective hydraulic conductivity, k_{max} (L/T) and k_{min} (L/T) are the lower and upper bound limits, $p(k)$ the frequency distribution function of hydraulic conductivity, n (dimensionless) is the number of dimensions, and k^* (L/T) is the conductivity for a homogeneous matrix.

- **Streamtube**

Streamtube is a method used to calculate the effective hydraulic conductivity of a sandy formation with the presence of shale, where horizontal shales can be considered barriers to vertical flow (Wen & Gómez-Hernandez, 1996). Begg & King (1985) developed a method that uses a distorted geometry of the actual streamlines to follow stream paths or tubes whose section is approximately rectangular. At the interior of each stream tube, the flow is calculated by solving the continuity equation (Emanuel et al., 1989; Hewett & Behrens, 1993). The selected number of streamlines must ensure that the geological medium is well sampled to represent the medium's heterogeneity (Begg et al., 1989). The vertical effective hydraulic conductivity can be estimated via:

$$K_v = \frac{(1-F_s)H^2}{N_s} \sum_{i=1}^{N_s} \frac{1}{S_i S_{ei}} \quad \text{(Eq. 2.10)}$$

where F_s (dimensionless) is the fraction of clay, N_s (dimensionless) the number of streamlines, S_i (L) the length of the ith streamline, S_{ei} (1/T) the length weighted by the permeability and H (L) the formation thickness.

2.3.2 Methods for scaling hydraulic conductivity to a tensor– porous medium

- **Simple Laplacian**

In the Simple Laplacian method, the aquifer is divided into blocks (grouping hydraulic conductivity from fine-scale), subsequently isolated to calculate the tensor components (Wen & Gómez-

Hernandez, 1996). For each block, the flow in x and y directions is calculated considering a priori that the direction of the main components of hydraulic conductivity and the main cartesian axes are parallel (Li et al., 2011a). Under the previous approach, the flow conditions and hydraulic head are parallel to the main directions of the block, and the hydraulic conductivity tensioner components in x and y directions are estimated using equations 2.11 and 2.12, respectively, in the case of a 2D problem (Li et al., 2011b).

$$K_{Vxx} = -\left(\frac{Q_x}{y_1 - y_0}\right) \div \left(\frac{h_1 - h_0}{x_1 - x_0}\right) \quad \text{(Eq. 2.11)}$$

$$K_{Vyy} = -\left(\frac{Q_y}{x_1 - x_0}\right) \div \left(\frac{h_1 - h_0}{y_1 - y_0}\right) \quad \text{(Eq. 2.12)}$$

where, Q_x and Q_y (L^3/T) are the flows through the cross-section of the block in a direction parallel to K_{Vxx} and K_{Vyy}, (L/T) respectively; h_1 and h_0 (L) represent the hydraulic heads; $x_1 - x_0$ and $y_1 - y_0$ (L) are the block size in a direction parallel to the flow, with which the simplified conductivity tensor Kv can be expressed as shown in equation 2.13:

$$Kv = \begin{bmatrix} K_{vxx} & 0 \\ 0 & K_{vyy} \end{bmatrix} \quad \text{(Eq. 2.13)}$$

The above approach is convenient when the parallelism between K (L/T) and Q (L^3/T) is fulfilled. However, the fine-scale hydraulic conductivity variability makes such a condition not necessarily valid for all cases.

- **Laplacian with skin**

As the Simple Laplacian, the Laplacian-with-skin method divides an area of interest in superblocks. The objective of the method is to estimate a full equivalent hydraulic conductivity tensor for each superblock. Assuming a full tensor eliminates the assumption of flow-conductivity parallelism within the superblock. The configuration of such superblocks is similar to the ones described previously for the Simple Laplacian. However, in this case, a thin skin (ring of cells) surrounds each superblock (Gómez-Hernández, 1991). The method generates a system of linear equations representing the flow conditions of all available superblocks. Skin cells act as local boundary conditions (prescribed heads, for example) of the local flow systems. By solving the linear system, it is possible to estimate the components of the hydraulic conductivity tensor.

Once the local flow systems solutions are available, the hydraulic head of the superblock h_V and specific flow of superblock block q_V values are determined by evaluating the following equations:

$$h_V(I,J) = \frac{1}{n_v} \sum_{(i,j)\epsilon V} h(i,j) \quad \text{(Eq. 2.14)}$$

$$q_V\left(I + \frac{1}{2}, J\right) = \frac{1}{n_l} \sum_{\left(i+\frac{1}{2}, j\right)\epsilon\, interface} q\left(i + \frac{1}{2}, j\right) \quad \text{(Eq. 2.15)}$$

where, n_v (dimensionless) is the numbered cell within the block, q (L^3/T) is the flow in cells, q_v (L^3/T) is the flow between blocks, and n_l (dimensionless) is the numbered cell at the borders of the neighboring blocks. With these heads and flows, it is possible to ensemble a system of linear equations for each superblock. These systems have the following mathematical form:

$$-\begin{bmatrix} (\partial h/\partial x)_1 & (\partial h/\partial y)_1 & 0 & 0 \\ 0 & 0 & (\partial h/\partial x)_1 & (\partial h/\partial y)_1 \\ \cdots & \cdots & \cdots & \cdots \\ (\partial h/\partial x)_n & (\mathrm{y})_n & 0 & 0 \end{bmatrix} \begin{bmatrix} K_{xx1} \\ K_{xy1} \\ \cdots \\ K_{yyn} \end{bmatrix} = \begin{bmatrix} q_{x1} \\ q_{y1} \\ \cdots \\ q_{xn} \\ q_{yn} \end{bmatrix} \quad \text{(Eq. 2.16)}$$

where, $(\partial h/\partial x)_i$ and $(\partial h/\partial y)_i$ (L) are the hydraulic gradient in x and y directions for the i^{th} block, and q_{xi} (L^3/T) and q_{yi} (L^3/T) are the flow in the i^{th} block in x and y direction, respectively. The system of equations 2.16 is generated by expressing the flow in the x and y directions for each block. These flows are functions of the hydraulic gradient and the components of the full hydraulic conductivity tensor. The unknown components of equation 2.16 are the scaling procedure products (H. Zhou et al., 2010). An essential advantage of the Laplacian-with-skin method, in comparison with the Simple Laplacian, is that it can produce upscaled tensors for very heterogeneous hydraulic conductivities. In theory, this flexibility enables its application in more realistic modeling problems, such as regional-scale studies.

2.3.3 Methods for scaling hydraulic conductivity of fractured medium either to a single value or to a tensor

- **Semi-Analytical and Semi-Analytical Superposition Methods**

The Semi-Analytical technique is based on analytical homogenization methods on which the fractures are modeled as thin ellipsoidal elements embedded in a rocky matrix with homogeneous hydraulic conductivity (Sævik et al., 2013). The upscaling procedure consists of calculating the effective hydraulic conductivity as:

$$K_e = \frac{4}{3}\pi f \sum_{i=1}^{N} \frac{\varepsilon_i}{\lambda_i}(I - n_i {n_i}^T) \quad \text{(Eq. 2.17)}$$

where, n_i is the vector normal to the fractures, f is the connectivity parameter that varies between 0 and 1, ε_i and λ_i are parameters for describing the density of fractures. Equation 2.17 was derived from Snow's methodology, which calculates the hydraulic conductivity tensor in fractured rocks having open fractures with infinite length. The parameter f was introduced by Oda (1985) to upscale hydraulic conductivity in a fractured rock where the extension of the fracture is finite.

The Semi-Analytica Superposition method considers the cubic law (Snow, 1969) as the basis for calculating the average velocity in the fracture plane and the different components of the hydraulic

conductivity tensor. These tensorial components are written as a function of the normal vector at the average of the discontinuity planes' orientation (Ababou et al., 1994; Chen et al., 1999; Kiraly, 1969). When the rock volume contains a single set of discontinuities with arbitrary orientation, the hydraulic conductivity tensor for the block can be estimated as:

$$[k_{ij}] = \frac{b^3}{12d}\begin{bmatrix} (n_2)^2 + (n_3)^2 & -n_1 n_2 & -n_3 n_1 \\ -n_1 n_2 & (n_3)^2 + (n_1)^2 & -n_2 n_3 \\ -n_3 n_1 & -n_2 n_3 & (n_1)^2 + (n_2)^2 \end{bmatrix} \quad \text{(Eq. 2.18)}$$

where, b (L) and d (L) are the fracture aperture and spacing, respectively, $n_1, n_2\ y\ n_2$ (dimensionless) are the components of the unit normal vector of the fracture plane. A general expression for calculating the components of the hydraulic conductivity tensor of a rock block on which the discontinuities can be grouped into sets where they can be considered parallel to each other is:

$$K_{ij} = \frac{g}{12v}\sum_{m=1}^{M} \frac{{A_m}^3}{L_m}\left(\delta_{ij} - n_{i,m} n_{j,m}\right) \quad \text{(Eq. 2.19)}$$

Where, g (L/T^2) is the acceleration of gravity, v (L^2/T) the kinematic viscosity, δ_{ij} the Kronecker delta and $n_{i,m} n_{j,m}$ (dimensionless) is the normal vector to the plane of the fracture.

- **Equivalent Porous Media**

The EPM method has been widely used for the regional modeling of groundwater flow in fractured rock. The method presumes the existence of a determined Representative Equivalent Volume (REV, see Figure 2), on which the small-scale variability of the hydraulic conductivity disappears. If it is possible to estimate the REV, an equivalent parameter or tensor represents the hydraulic conductivity variability due to the rock's discontinuities (Bear et al., 1993; Berkowitz et al., 1988; Long et al., 1982). With the previous considerations, the REV represents the minimum model block size for which applying the EPM method is valid when simulating groundwater flow in rocks. The effective hydraulic conductivity can be estimated using one of the methods previously discussed in the paper.

To calculate the hydraulic conductivity tensor with the EPM approach, the flow through the fracture network is simulated with the DFN method, evaluating hydraulic gradients in the x and y directions for different scales. The flow simulations are carried out until reaching the REV (see Figure 2).

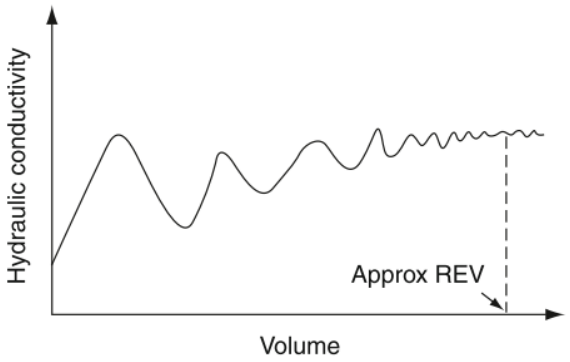

Figure 2. Variation of hydraulic conductivity as a function of the volume of rock. Taken from (Singhal & Gupta, 2010)

Figure 2 shows the variability of hydraulic conductivity as a function of the rock volume. Hydraulic conductivity varies widely for rock sizes less than REV, while for rock volumes bigger than the representative volume, the variability of hydraulic conductivity is considered negligible (Singhal & Gupta, 2010).

2.4 Conclusions

In this article, we have reviewed different techniques for scaling hydraulic conductivity. The usefulness of such techniques is that, through their use, it is possible to implement groundwater flow models on a much larger scale than the scale of measurement of hydraulic conductivity. We have presented techniques that produce a single scaled block value and techniques that produce an equivalent tensor. We conclude that the techniques that produce tensors are promising for scaling rocky media in regional applications.

Within the techniques presented in section 2.3, we consider that two types of techniques can be used for scaling the hydraulic conductivity in a fractured medium. The first type corresponds to the Semi-Analytical and Semi-Analytical Superposition techniques. They calculate the effective hydraulic conductivity or the block tensor components from the fractures' geometric parameters and the rocky matrix's hydraulic conductivity. In the second group, we include the EPM approach and the Laplacian with skin technique. Out of these techniques, we consider the use of Laplacian-with-skin to be promising for scaling hydraulic conductivity in fractured media. It allows us to consider in more detail the variability of fine-scale hydraulic conductivity within the block.

In the last ten years, authors such as (Fu et al., 2011; Li et al., 2010, 2011a, 2011b, 2012; Llerar-Meza, 2009; H. Zhou et al., 2010) have presented applications and modifications of the Laplacian with skin from (Gómez-Hernández, 1991). However, all the works have been focused on scaling the hydraulic conductivity of heterogeneous porous media. From the detailed review of the

Laplacian-with-skin method's operation, we consider that it can be used to scale the hydraulic conductivity of fractured media if the fractures network is adequately represented on a fine-scale of hydraulic conductivity. Therefore, in chapter 3, we evaluate the Laplacian-with-skin method's applicability in fractured media, scaling on hydraulic conductivity fields similar to that shown in Figure 1.

3 Calculation of Hydraulic Conductivity Tensor in 2D Applying Laplacian with Skin to Fractures Network

Harol Alexander Cetre-Orejuela, Marcela Jaramillo, Oscar David Álvarez-Villa

Abstract: Treatment of fractured medium as a continuum through equivalent hydraulic parameters has proven to be a suitable approach for flow and mass transport modeling in a large-scale fractured media. In this article, we present one way to calculate the equivalent hydraulic conductivity tensor for blocks of regional flow models through scaling, based on the rock's fractures' geometry characteristics. Our method operates as follows: (i) the probability distribution functions (pdf) of the DFN are parameterized using measurements of fracturing parameters, (ii) DFN are generated, (iii) Laplacian with skin is applied, and hydraulic conductivity tensors for blocks in the coarse-scale are obtained, (iv) the model is run solving the groundwater flow equation with the complete hydraulic conductivity tensor. We applied this method to a 2D synthetic fractured medium and found that the scaled models adequately represent fine-scale hydraulic heads, but to some extent. There is a block size in the coarse-scale for which the variability of the hydraulic conductivity is too homogenized, and the scaled models lose precision in the representation of the fine-scale heads.

3.1 Introduction

The Discrete Fracture Network (DFN) technique is one of the most widely used for modeling groundwater flow in fractured media (Cacas et al., 1990). Since the DFN method focuses on representing the flow within the individual fractures in the rock matrix, its application at the regional scale has been relatively limited. Three main reasons explain the lack of using the DFN method in regional groundwater flow modeling. First, it is difficult to measure the required hydraulic properties of the individual fractures to parameterize the models (Scanlon et al., 2003). Second, the DFN technique explicitly considers the connectivity amongst individual fractures, which causes a considerable computational burden for highly discretized models covering broad areas (Young et al., 2019). Third, despite advances in computer processing capacity, it is impossible to model

the groundwater flow in all fracture network elements realistically due to the impossibility of measuring hydraulic conductivity at all the individual components (Renard & de Marsily, 1996). In general, DFN models have been used to determine the fractures network's equivalent hydraulic parameters and recreate flow observations in fractures at a site (Neuman, 2005).

Due to the above limitations of the DFN method, most of the groundwater flow modeling applications, at the regional scale, use the Equivalent Porous Media approach. The EPM method represents the fractured rock as an equivalent porous medium. It is, then, possible to determine a set of equivalent parameters that resemble the original flow conditions in the rock (Anderson et al., 2015; Long et al., 1982).

In this paper, we explore the viability of applying the Laplacian with skin technique (Gómez-Hernández, 1991) to upscale hydraulic conductivities in the fractured medium. Our objective is to show that using tensor-based upscaling techniques, such as the Laplacian with skin, and the EPM approach would allow implementing more efficient regional groundwater flow models. For such an end, we generated a synthetic two-dimensional fractured media with its respective hydraulic conductivity field. This field is representative of the small (sampling) scale. The fractured network is generated using the Priest (1993) method with fracture parameters sampled from the Dunita of Medellin geological unit. Each fracture's hydraulic conductivity is calculated using the cubic law (Witherspoon et al., 1980). Our method does not calculate a single equivalent value of hydraulic conductivity on the REV scale. Instead, we calculate a tensor for accounting more accurately for the fine-scale variability of the hydraulic conductivity.

3.2 Theoretical Framework

In this section of the article, we present the theoretical framework used to implement the hydraulic conductivity scaling algorithm and calculate the conductivity tensor.

3.2.1 Groundwater flow equation and Finite Difference method

By combining the continuity and momentum conservation (Darcy's law) equations, the steady-state groundwater flow equation in saturated porous media subject to boundary conditions can be expressed as (Bear & Cheng, 2010).

$$\frac{\partial}{\partial x}\left(K_{xx}\frac{\partial h}{\partial x}+K_{xy}\frac{\partial h}{\partial y}\right)+\frac{\partial}{\partial y}\left(K_{yy}\frac{\partial h}{\partial y}+K_{yx}\frac{\partial h}{\partial x}\right)+W(x,y)=0 \quad \text{(Eq. 3.1)}$$

where, x and y are the cartesian coordinates, h (L) is the hydraulic head, K_{xx}, K_{yy}, and K_{xy} (K_{xy}=K_{yx}) (L/T) are the component of the symmetric hydraulic conductivity tensor, and $W(x,y)$ are the external stresses.

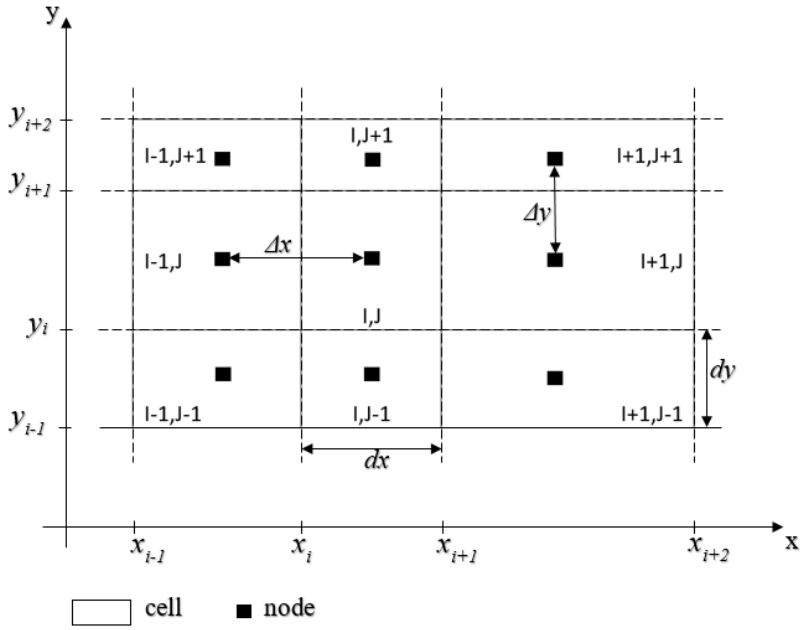

Figure 3. Nine-point discretization scheme used for the approximation of the hydraulic head of the equation 3.1 using the Finite Difference method. In the notation of the figure, the subscript I indicates the position of a cell concerning the x direction and J to the y direction. Δx_i and Δy_i represent the separation between two cell nodes in the x and y directions, and dx_i and dy_i are the width of the cells for x and y directions, respectively. Adapted from (Gómez-Hernández, 1991).

The solution of equation (3.1) using the Finite Difference method (FD) for irregularly spaced nodes is given by the central approximations of each component of the spatial derivatives. The approximations are obtained from the analysis of the nine-point scheme of Figure 3, where the partial derivatives of second order that accompany the hydraulic conductivity components K_{xx} and K_{yy}, can be calculated via:

$$\frac{\partial}{\partial x}\left(K_{xx}\frac{\partial h(x,y)}{\partial x}\right) \approx \frac{1}{(d_x)_{I,J}}\left[K_{xx(I+1,J)}\frac{h_{I+1,J}-h_{I,J}}{(\Delta_x)_{I+1,J}} - K_{xx(I-1,J)}\frac{h_{I,J}-h_{I-1,J}}{(\Delta_x)_{I-1,J}}\right] \quad \text{(Eq. 3.2)}$$

$$\frac{\partial}{\partial y}\left(K_{yy}\frac{\partial h(x,y)}{\partial y}\right) \approx \frac{1}{(d_y)_{I,J}}\left[K_{yy(I,J+1)}\frac{h_{I,J+1}-h_{I,J}}{(\Delta_y)_{I,J+1}} - K_{yy(I,J-1)}\frac{h_{I,J}-h_{I,J-1}}{(\Delta_x)_{I,J-1}}\right] \quad \text{(Eq. 3.3)}$$

Moreover, the approximation for the terms of the partial second-order derivatives that accompany the conjugate components are:

$$\frac{\partial}{\partial x}\left(K_{xy}\frac{\partial h(x,y)}{\partial y}\right) \approx \frac{1}{(d_x)_{I,J}}\left[K_{xy}\frac{\partial h(x,y)}{\partial y}\Big|_{I+1,J} - K_{xy}\frac{\partial h(x,y)}{\partial y}\Big|_{I-1,J}\right] \quad \text{(Eq. 3.4)}$$

$$\frac{\partial}{\partial y}\left(K_{xy}\frac{\partial h(x,y)}{\partial x}\right) \approx \frac{1}{(d_y)_{I,J}}\left[K_{xy}\frac{\partial h(x,y)}{\partial x}\Big|_{I,J+1} - K_{xy}\frac{\partial h(x,y)}{\partial x}\Big|_{I,J-1}\right] \quad \text{(Eq. 3.5)}$$

where, $d_{x_{I,J}}$ (L) and $d_{y_{I,J}}$ (L) are the width in x and y direction for the cell, Δ_x (L) and Δ_y (L) are the separation between nodes centers of two cells in the x and y directions, respectively, $K_{xx_{(I+1,J)}}$ (L/T) is the hydraulic conductivity inter cells (I,J) and $(I+1,J)$, $K_{xx_{(I-1,J)}}$ (L/T) inter cells (I,J) and $(I-1,J)$, $K_{yy_{(I,J+1)}}$ (L/T) inter cells (I,J) and $(I,J+1)$, and $K_{yy_{(I,J-1)}}$ (L/T) inter cells (I,J) and $(I,J-1)$. Expanding equation (3.4) and equation (3.5) and substituting in them the centered approximations of the first-order spatial derivatives that accompany the conjugate components of hydraulic conductivity, we obtain that:

$$\frac{\partial}{\partial x}\left(K_{xy}\frac{\partial h(x,y)}{\partial y}\right) \approx \frac{1}{(d_x)_{I,J}}\left[\left(\frac{k_{xy(I-1,I)}(h_{I-1,J+1}-h_{I-1,J-1})}{(\Delta_y)_{J+1,J}+(\Delta_y)_{J,J-1}}\right) - \left(\frac{k_{xy(I,I+1)}(h_{I+1,J+1}-h_{I+1,J-1})}{(\Delta_y)_{J+1,J}+(\Delta_y)_{J,J-1}}\right)\right] \quad \text{(Eq. 3.6)}$$

$$\frac{\partial}{\partial y}\left(K_{xy}\frac{\partial h(x,y)}{\partial x}\right) \approx \frac{1}{(d_y)_{I,J}}\left[\left(\frac{k_{xy(J+1,J)}(h_{I-1,J+1}-h_{I+1,J+1})}{(\Delta_x)_{I-1,I}+(\Delta_x)_{I,I+1}}\right) - \left(\frac{k_{xy(J-1,J)}(h_{I-1,J-1}-h_{I+1,J-1})}{(\Delta_x)_{I-1,I}+(\Delta_x)_{I,I+1}}\right)\right] \quad \text{(Eq. 3.7)}$$

where $K_{xy(I-1,I)}$ (L/T) is the conjugate hydraulic conductivity inter cells $(I-1,J)$ and (I,J), $K_{xy(I,I+1)}$ (L/T) inter cells (I,J) and $(I+1,J)$, $K_{xy(J+1,J)}$ (L/T) inter cells $(I,J+1)$ and (I,J), and $K_{xy(J-1,J)}$ (L/T) inter cells (I,J) and $(I,J-1)$.

3.2.2 Generation of the fractures network

Before testing the hydraulic conductivities upscaling methods, it is necessary to create a fine-scale fractured medium. We assume that such a medium contains two groundwater flow domains: the semi-permeable fresh rock and the fractures network. DFN generators can simulate fracture networks as a function of geometric parameters (Jing & Stephansson, 2007; Ren et al., 2017). Orientation (dip, dip direction, and strike), spacing (frequency), aperture, continuity (fracture size), and shape are the parameters of interest (Singhal & Gupta, 2010). DFN generators use probability distributions to describe the fracture parameters' statistical variability (Lei et al., 2017). By sampling such distributions, it is possible to map equally plausible fracture networks (Min et al., 2004). In the following, we describe the procedure for statistically characterizing the geometric parameters of the fractures.

First, let us suppose that we have a set of fracture parameters samples. From this set, we extract a predefined number of characteristic subsets (fractures families), for which we estimate the central trend (mean) and dispersion statistics (standard deviation). We must now fit the deviations of the normal vector of each discontinuity with the normal mean vector of the respective family

(Priest, 1993). The probability distribution function used to adjust the orientation data is the Fisher function (Fisher, 1953), shown in equation 3.8.

$$P(\theta) = \eta e^{Kcos\theta} d\theta \quad \text{(Eq. 3.8)}$$

where, K (dimensionless) is a constant that controls the shape of the distribution, and η (dimensionless) is a variable that ensures that the sum of all the possible values of $p(\theta)$ is 1.

Second, we assume that the spacing, continuity, and opening follows a determined probability distribution. These probability functions were selected based on the distribution of the geometric variables of each set of fractures. To determine which of the theoretical functions represents better the data distribution, the Smirnov-Kolmogorov test was used with a significance level of 0.05. Table 1. describes the selected theoretical distribution functions for the statistical modeling of the fractures' opening, size, and spacing.

Table 1. Theoretical distributions of the parameters

Distribution	Expression	Parameters
Log-Normal 2	$f(x) = \frac{1}{x\sigma\sqrt{2\pi}} e^{-\frac{1}{2}\left(\frac{\ln(x)-\mu}{\sigma}\right)^2}$	μ and σ are the mean and standard deviation
Log-Normal 3	$f(x) = \frac{1}{(x-\Upsilon)\sigma\sqrt{2\pi}} e^{-\frac{1}{2}\left(\frac{\ln(x-\Upsilon)-\mu}{\sigma}\right)^2}$	μ and σ are the mean and standard deviation, and ϒ is a location parameter
Exponential 1	$f(x) = \lambda e^{-\lambda x}$	λ is the average value of occurrences
Exponential 2	$f(x) = \lambda e^{-\lambda(x-\Upsilon)}$	λ is the average value of occurrences ϒ is a location parameter

Finally, it is possible to generate stochastic equally plausible realizations of fracture networks via Monte-Carlo simulation. These realizations honor the available data and the respective fitted theoretical distribution. Priest (1993) presents in detail the procedure for generating the 2D and 3D DFN models.

3.2.3 Laplacian with skin

The Laplacian with skin (Gómez-Hernández, 1991) is an upscaling technique that transforms hydraulic conductivity estimates at the small-scale to the large scale. In the following, we describe in detail this upscaling procedure. Let us assume that we have a hydraulic conductivity field at a small scale. We overlap a coarse mesh of superblocks to this field, intending to estimate equivalent tensors of hydraulic conductivity. These tensors intend to represent, as well as

possible, the smaller scale groundwater flow in the superblock. With this in mind, it is necessary to solve repeatedly the groundwater flow equation (3.1) for each superblock surrounded by a thin skin of cells. Figure 4 presents the geometric configuration of the characteristic domain for the upscaling procedure.

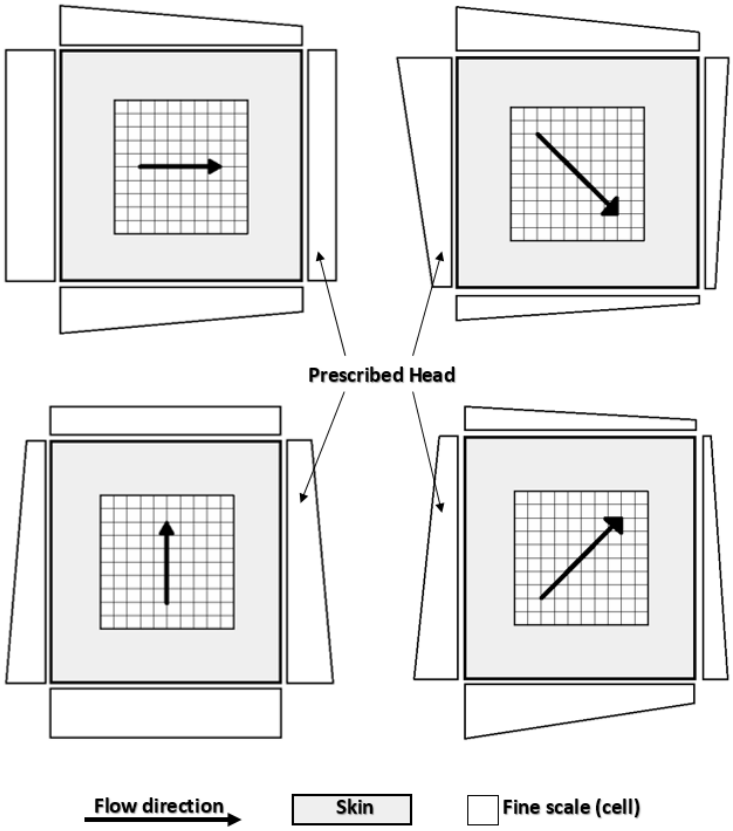

Figure 4. Local flow systems for calculating hydraulic heads and specific flows in blocks. Membrane or skin around the block is formed by cells and hydraulic head as boundary conditions for the local system solution. The prescribed hydraulic heads are strategically located to determine the flow in a particular orientation. The skin is a set of auxiliary cells that attenuate the effect of the boundary conditions used in each local model during the flow problem's solution—source: Adapted from (Wen & Gómez-Hernandez, 1996).

The groundwater flow problem for each superblock consists of a rectangular area surrounded by a predefined number of cells used for mitigating the impact of the boundary conditions in the representation of the flow dynamics in the superblock. Figure 4 shows different geometries of prescribed heads boundary conditions. The geometric properties of such conditions are key because they control: (i) the predominant flow direction in the superblock, (ii) the local flow velocities, and (iii) the magnitudes of the estimated components of the hydraulic conductivity tensor. (Li et al., 2011a, 2011b). The equivalent superblock hydraulic conductivity is the amount

that relates the average value of the cell-specific fluxes between adjacent blocks to the hydraulic gradient between blocks, as follows:

$$\frac{1}{V}\int_V \bar{q}dV = -K_V\left(\frac{1}{V}\int_V \nabla\bar{h}dV\right) \quad \text{(Eq. 3.9)}$$

where, K_v (L/T) is the hydraulic conductivity of the block, V (L^3) is the volume or size of the block, h (L) is the hydraulic head of cells, and q (L^3/T) is the flow in cells. After solving the local groundwater flow problems, it is possible to calculate the hydraulic head, h_V (L), and the average flows q_V (L^3/T), in each block, as (Wen & Gómez-Hernandez, 1996):

$$h_V(I,J) = \frac{1}{n_v}\sum_{(i,j)\epsilon V} h(i,j) \quad \text{(Eq. 3.10)}$$

$$q_V\left(I+\frac{1}{2},J\right) = \frac{1}{n_l}\sum_{\left(i+\frac{1}{2},j\right)\epsilon\, interface} q\left(i+\frac{1}{2},j\right) \quad \text{(Eq. 3.11)}$$

where, $h(i,j)$ (L) is the hydraulic head in fine scale, h_V (L) is the average hydraulic head in the superblock, n_V (dimensionless) is the number cell within the superblock, q (L^3/T) is the flow in the cells at a local scale, q_V is the flow between superblocks and n_l (dimensionless) is the number of cells that make up the border between neighboring blocks. After estimating the h_V (L) and q_V (L^3/T), the inter-superblock flows are expressed as a function of the gradients and the superblock's hydraulic conductivities. By applying the generalized Darcy's Law for all the superblocks, the following overdetermined system of linear equation results:

$$-\begin{bmatrix} (\partial h/\partial x)_1 & (\partial h/\partial y)_1 & 0 & 0 \\ 0 & 0 & (\partial h/\partial x)_1 & (\partial h/\partial y)_1 \\ \cdots & \cdots & \cdots & \cdots \\ (\partial h/\partial x)_n & (\partial h/\partial y)_n & 0 & 0 \end{bmatrix}\begin{bmatrix} K_{xx1} \\ K_{xy1} \\ \cdots \\ K_{yyn} \end{bmatrix} = \begin{bmatrix} q_{x1} \\ q_{y1} \\ \cdots \\ q_{xn} \\ q_{yn} \end{bmatrix} \quad \text{(Eq. 3.12)}$$

where, $(\partial h/\partial x)_i$ and $(\partial h/\partial y)_i$ (L) are the hydraulic gradient in x and y directions for the i^{th} block; q_{xi} (L^3/T) and q_{yi} (L^3/T) are the flow in the i^{th} block in x and y direction. The unknown quantities of the system (3.12) are the components of the hydraulic conductivity tensor. By solving such an equation, we obtain the different components of the upscaled hydraulic conductivity tensors. In other words, equation (3.12) is the upscaling law for the Laplacian-with-skin method.

3.3 Methods

In this section, we present a methodology to upscale hydraulic conductivity in a fractured medium. Our technique integrates the generation of a DFN and the full groundwater flow equation solution

via finite differences and the Laplacian with the skin upscaling method. We implemented this algorithm in a Python 3.7 script for two-dimensional rectangular aquifers.

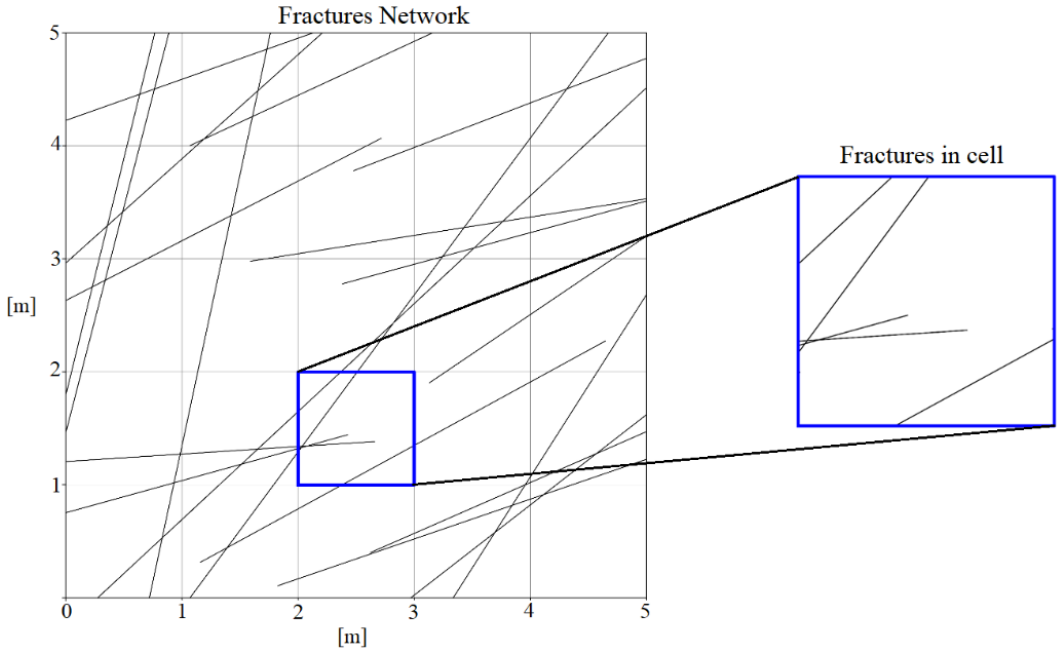

Figure 5. Identification of fractures inside cells for the calculation of the K_{xx} and K_{yy} components of the hydraulic conductivity tensor on the fine-scale. Own elaboration.

We apply the upscaling procedure for a two-dimensional fractured medium. As the first step of the scaling procedure, we create a realization of DFN using the method described in subsection 3.2.2. Then, we discretize the modeling area into squared cells and apply a moving window algorithm to the DFN, as shown in Figure 5. This algorithm allows us to build the fine-scale of hydraulic conductivities, identifying the existence of families of fractures within each cell and calculating the value of hydraulic conductivity for each cell depending on the families of fractures within it.

The moving window algorithm works as follows: First, we define the window size equal to the fine-scale cell size. After we calculate the number of movements that the window must make to cover the entire domain of the fractures network, we estimate the hydraulic conductivity of the fractures, and build the fine-scale. We calculate the number of movements as the ratio between the fractures network's domain area and the window area. In each movement, the window evaluates the existence of fractures in its interior, based on the coordinates of the fractures' initial and final points (Figure 6).

The three schemes shown in Figure 6 comprise one single diagram. However, we present the schemes individually to avoid saturation of the image and make it legible. In the three diagrams, the continuous black lines represent the fractures, and the black points represent the beginning

and end of these fractures. The discontinued red lines demarcate the areas where the fractures' extreme points vary, either inside or outside the window. The gray shaded rectangle represents the moving window. The arrangement of the black lines concerning the window outlines the possible ways in which a fracture may be intercepted by the window, as follows: (i) a fracture may be contained entirely within the window, (ii) a fracture can be intercepted by the window and have one extreme point in the inside of the window and the other extreme point in the outside, (iii) a fracture can be intercepted by the window and its extreme points be outside the window. Cases (i) and (ii) describe the 10-point scheme of Figure 6, while case (iii) describes the 8 and 6 points schemes.

It should be noted that, in each movement of the windows, it can intercept one, several, or no fractures; in the latter case, the location of the fracture concerning the window does not correspond to any of the possible arrangements indicated in the 10, 8 and 6 point diagrams. Then, the algorithm assigns a rock matrix hydraulic conductivity value to the fine-scale cell.

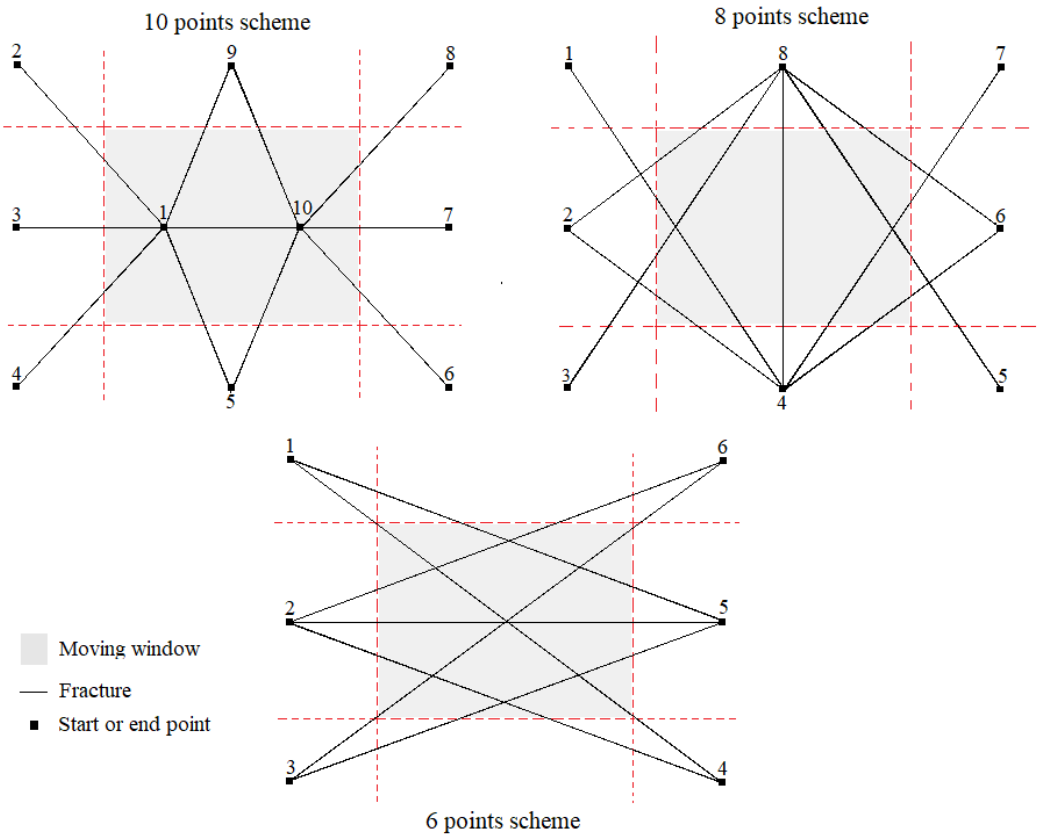

Figure 6. Schemes of 10, 8, and 6 points for calculating sections of fractures intercepted by the mobile window. Own elaboration.

We calculate each cell's hydraulic conductivity that contains fractures using the cubic law of Snow (1969) (eq. 3.13), depending on the fractures' opening and the number and type of fractures within of window.

$$K_{fi} = \frac{gb^3}{12\nu} \quad \text{(Eq. 3.13)}$$

where, b (L) is the aperture of the fracture, g (L/T^2) is the gravitational acceleration, and ν (L^2/T) is the kinematic viscosity. We assume that, at the local fracture scale, the components K_{xx} and K_{yy} (L/T) of the hydraulic conductivity tensor are equal and constant along the fracture plane.

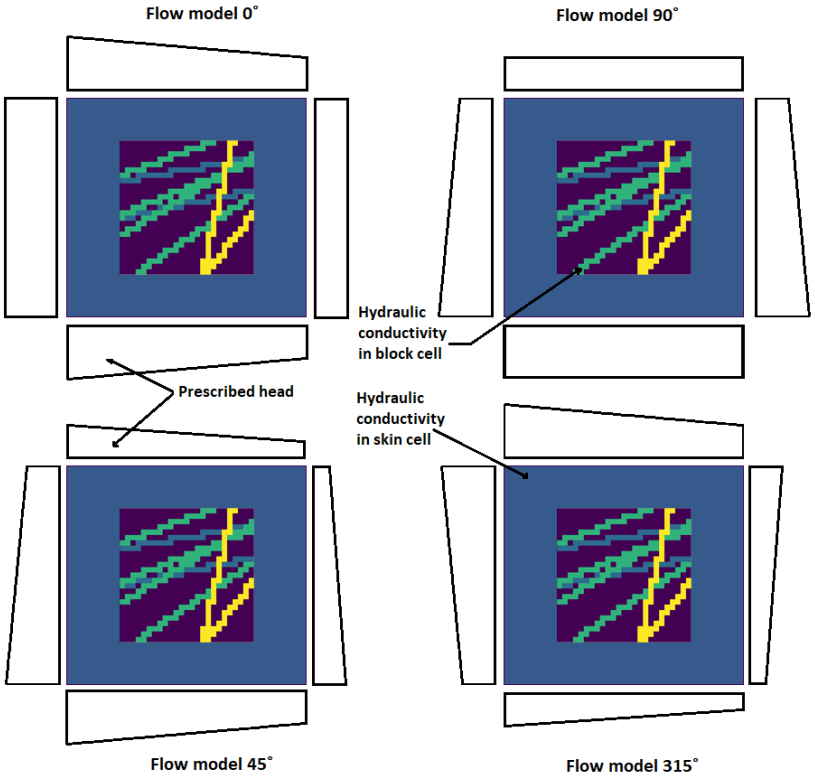

Figure 7. Local flow models for calculating hydraulic heads and specific flows in blocks representing the field of hydraulic conductivity from fracture network. The heterogeneous medium on which the local flow models are solved corresponds to a fractures network represented with a finely discretized hydraulic conductivity field—adapted from (Wen & Gómez-Hernandez, 1996).

After constructing the fine-scale hydraulic conductivity field using the moving window technique, we apply the Laplacian-with-skin method as explained previously in subsection 3.2.3. Unlike the traditional Laplacian with skin application to a porous medium, we build local models with hydraulic conductivity fields that explicitly represent the fracture network, as shown in Figure 7.

Figure 8 depicts the main steps in our upscaling methodology. As commented previously, this algorithm consists basically of three steps. The first step is the statistical description of the fracture

network (see green square). The second step is the generation of the DFN and the estimation of the small-scale hydraulic conductivity (see blue square). The last step is the upscaling of the hydraulic conductivity at the coarse block scale via the Laplacian-with-skin method (see red square). Our scaling method requires information on orientation, spacing, aperture, continuity, and shape. Sampling these parameters is a common practice of field geology for the structural characterization of the rocks. The methodology also requires the definition of the superblock size, the skin width, and the prescribed heads for each block. The Smirnov-Kolmogorov tests for selecting the theoretical probability distributions function (pdf) of such parameters should be performed previously to the DFN generation. The output of our methodology is three upscaled hydraulic conductivity fields. Each field represents the different components of the full tensor.

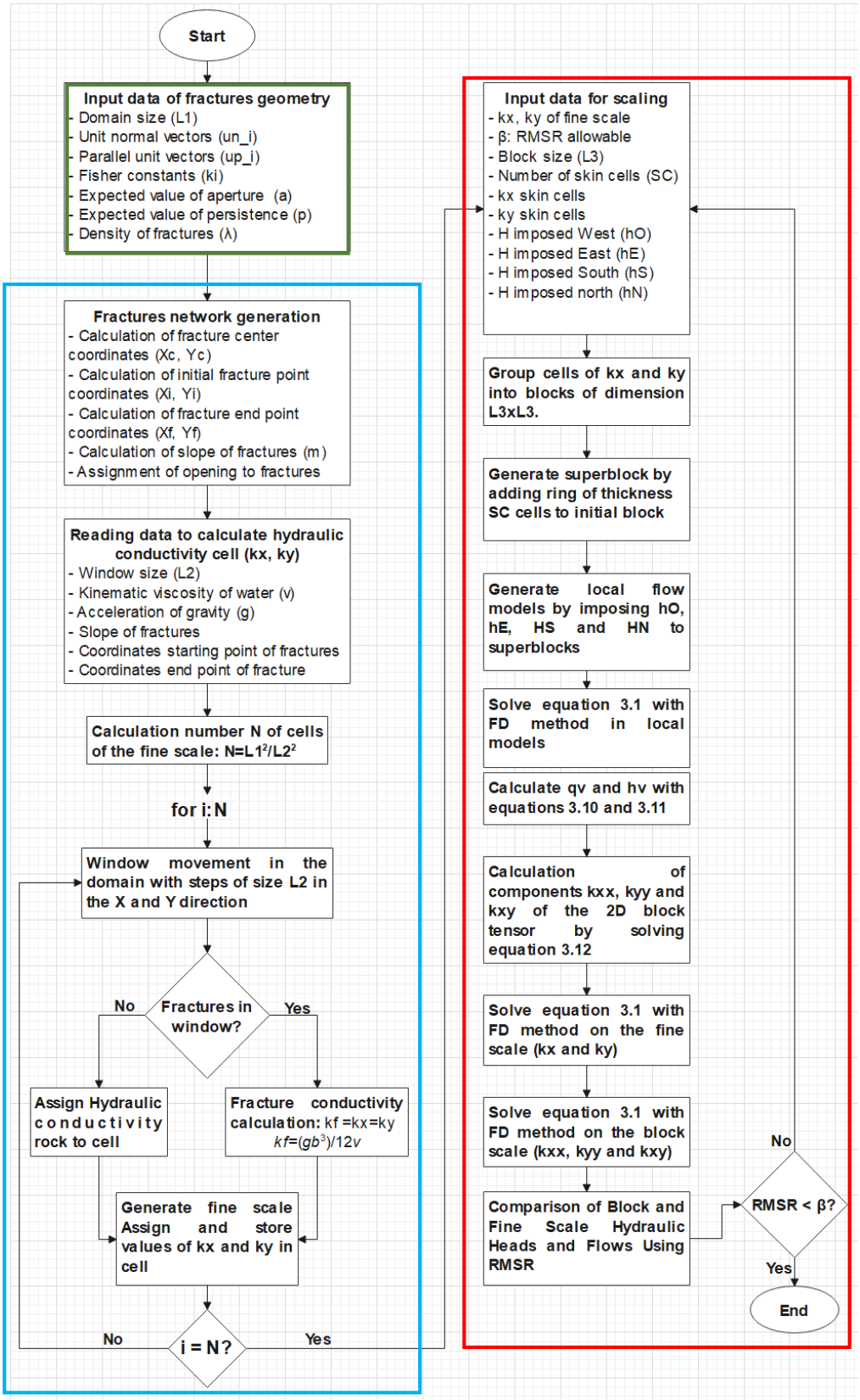

Figure 8. Flow chart with the structure of the hydraulic conductivity scaling algorithm. Own elaboration.

We test the capabilities of our methodology in a synthetic example. To evaluate whether the scaling process reproduces the average dynamics of the groundwater flow at the fine scale, we use different performance metrics such as (i) the mean squared error, (ii) residual histograms, and (iii) descriptive statistics of the residuals of the fine-coarse scale heads.

3.4 Data

We used the fracture parameters sampled in the Medellin Dunite geological unit (JkuM) (Patiño et al., in prep.) to simulate the reference DFN, to estimate the fine-scale hydraulic conductivity, and to test our hydraulic conductivity upscaling methodology. The Medellin Dunite is part of the Aburrá Ophiolithic complex that corresponds to a strip of ultramafic rocks. The Dunite is an elongated body in the N10°W direction that emerges in the east of the Aburrá Valley between the municipalities of Medellín, Envigado, and the town of Santa Elena, in the department of Antioquia, Colombia.

The available data consists of 1086 sets of discontinuity data at 51 stations, including fractures, joint, and faults parameters: dip, dip direction, persistence or continuity, opening, filling, roughness, weathering, and the spacing between fractures. The Undergraduate Groundwater Research Group (SIAS by its Spanish acronym) of the Geology program at the Department of Earth Sciences of EAFIT University collected this information during April and October of 2019. From a geostatistical analysis, Patiño et al. (in prep) identified six fracture families as a function of the statistical similarity in the dip and dip direction parameters. Table 2. presents each family's main statistical characteristics: number of observations, the percentage of data (regarding the whole data set), the average dip-direction, and the average dip-set.

Table 2. Set of discontinuities used in the modeling of the discontinuities of the Dunita of Medellín.

Discontinuity set	Data set	Percentage	Dip direction – set (°)	Dip – set (°)
F1	175	16,11	156	26
F2	153	14,09	186	55
F3	217	19,98	258	54
F4	145	13,35	031	69
F5	238	21,92	115	71
F6	158	14,55	324	63

Figure 9 depicts the estimated histograms of fracture parameters for each data subset. Plots (A) present the histograms estimated for fracture spacing, plots (B) present the histograms for fracture size (length), and plots (C) present histograms for fracture opening. All these histograms represent

the approximate form of the six families of fractures' distribution function, grouped based on the statistical similarity of the dip and dip direction parameters. Table 3. , Table 4. , and Table 5. present the univariate descriptive statistics of fracture spacing, size, and opening of all previously defined fracture families.

For all the six families of fractures (Figure 9A), the spacing histograms are skewed, with at least 50% of the data grouped in the first two ranges of the histograms. In particular, more than 75% of the spacing observations in family F5 are less than the average spacing. Similarly, approximately 50% of the spacing samples are less than the average for families F2, F3, F4, and F6. Interestingly, the estimated average spacing of the family F1 is less than the median, which could mean some atypically low observations in the dataset (see Table 3.).

In the fracture size histograms (Figure 9B), Families F2, F3, F4, F5, and F6 show positively skewed distributions. In this regard, 36% of the observed sizes in the family F1 are in the range of 2.5 m and 3 m. Family F1 shows a smaller fracture size bias than the other five fracture families (skew coefficient of 0.01, see Table 4.). In families F2, F3, F4, F5, and F6, the average fracture size is greater than 50% of the available samples. The opposite situation occurs in the F1 family, where the mean size of the fractures (1.81 m) is lower than the median (2.00 m) of the measurements (see estimated mean and median in Table 4.). The coefficient of variation estimated for the fracture sizes of family F1 is 0.63. This statistic is slightly larger for the other families, with estimates from 0.84 to 0.88 (see estimates in Table 4.). Although the degree of dispersion of all fracture size subsamples is similar, these dispersions are relatively large. This result denotes the existence of a marked statistical variability of the fracture family sizes.

The fracture opening's empirical distributions for all the families show positive bias (see histograms (C) in Figure 9). It is essential noticing that the shapes of such distributions are similar to a negative exponential distribution function. In general, at least 80% of the available opening data are in the range [0,0 mm, 5,0 mm] (see Table 5.). Besides, all the six estimated average openings are greater than 75% of the respective available samples. This result means that most of the observations are concentrated in the lower tail of the empirical distributions. Also, it implies that there are some outliers or anomalous observations in the data sets. The anomalous openings correspond to discontinuities caused by the mineral dissolution of brucite during the Medellin Dunite's chemical weathering. The opening data used in this statistical characterization was sampled directly on the discontinuities. Since we lack hydraulic tests, we assume that these observations are representative of the hydraulic opening of the fractures for the whole geological unit.

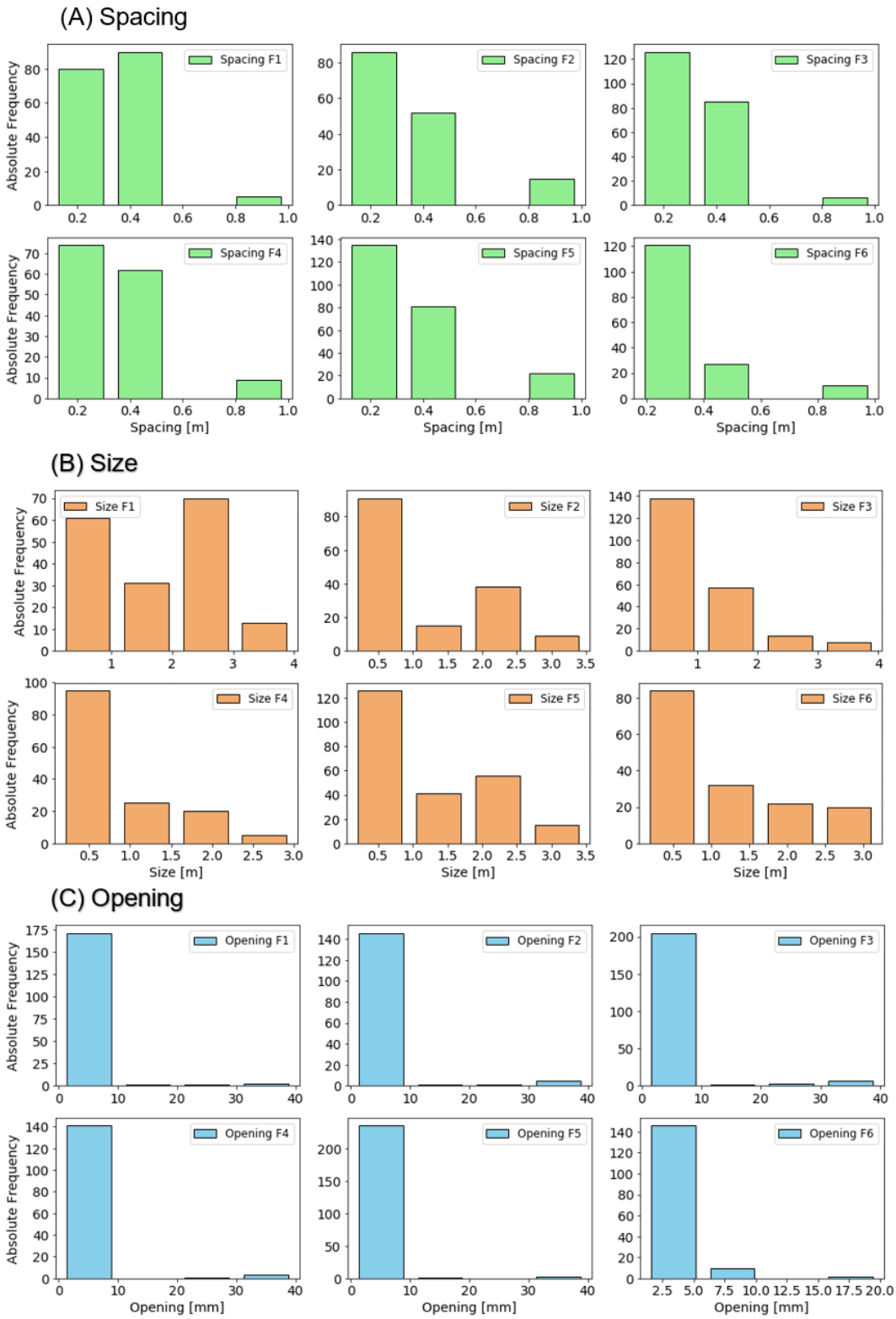

Figure 9. Absolute frequency histogram of fracture (A) spacing, (B) size, and (C) Opening, grouped based on the statistical similarity of the dip and dip direction parameters. Own elaboration.

Table 3. Univariate statistics of the spacing measurements of the six discontinuity sets of Medellin Dunite.

Spacing	F1	F2	F3	F4	F5	F6
Min (m)	0,10	0,10	0,10	0,10	0,10	0,17
Max (m)	1,00	1,00	1,00	1,00	1,00	1,00
Mean (m)	0,30	0,36	0,31	0,32	0,34	0,35
Quartile 1 (m)	0,25	0,25	0,20	0,20	0,20	0,25
Median (m)	0,33	0,25	0,25	0,25	0,25	0,29
Quartile 3 (m)	0,33	0,50	0,33	0,33	0,33	0,33
Stand dev (m)	0,16	0,24	0,16	0,21	0,24	0,20

Table 4. Univariate statistics of fracture size measurements for the six discontinuity sets of Medellin Dunite.

Size	F1	F2	F3	F4	F5	F6
Min (m)	0,12	0,10	0,10	0,12	0,10	0,10
Max (m)	4,00	3,50	4,00	3,00	3,50	3,20
Mean (m)	1,81	1,05	0,98	0,84	1,08	1,10
Quartile 1 (m)	0,68	0,28	0,30	0,25	0,30	0,26
Median (m)	2,00	0,68	0,65	0,50	0,80	0,80
Quartile 3 (m)	2,60	2,00	1,40	1,40	1,80	1,78
Stand dev (m)	1,15	0,93	0,87	0,71	0,88	0,93

Table 5. Univariate statistics of fracture opening measurements for the six discontinuity sets of Medellin Dunite.

Opening	F1	F2	F3	F4	F5	F6
Min (mm)	0,10	0,10	0,40	0,10	0,10	1,00
Max (mm)	40,00	40,00	40,00	40,00	40,00	20,00
Mean (mm)	3,07	3,65	3,99	3,55	2,67	1,90
Quartile 1 (mm)	1,00	1,00	1,00	1,00	1,00	1,00
Median (mm)	1,00	1,00	1,00	1,00	1,00	1,00
Quartile 3 (mm)	2,00	3,00	2,00	3,00	2,00	1,00
Stand dev (mm)	5,37	7,52	7,92	6,52	4,47	2,79

Finally, for estimating the hydraulic conductivity of the DFN, we make two assumptions due to the lack of data. First, we neglect the effect of the fracture roughness in the generation of the DFN parameters. Nevertheless, previous works show that this consideration does not affect the simulated flows within the fractures significantly. Furthermore, assuming smooth equivalent fracture is common in the DFN models (Jing & Stephansson, 2007). Second, we assume that some specific geologic structures control the hydraulic behavior of the fracture network. In particular, we neglect the effect of large-scale geological structures, such as faults or fracture zones whose extension can span kilometers. Likewise, we neglect the effect of microscale

structures on the hydraulic characteristics of the fractured rock. Fractures at this scale control the primary porosity of the rock matrix. Representing in detail this kind of variability is not the scope of this work. With this in mind, we are interested in representing structures such as fractures, joints, foliations, among others. This kind of discontinuities controls the secondary porosity of the rock and configures the fracture network.

3.5 Results analysis and discussion

This section presents and analyzes the results obtained by applying our scaling methodology to the fracture measurements on the Medellin Dunite. First, we illustrate the main features of the theoretical pdf fitted to the geometric parameters of the fractures mapped in the Dunita de Medellín. We use these pdfs to generate the DFN at the fine scale, to which we apply the upscaling technique. Second, we present the hydraulic conductivity fields estimated at the fine-scale for the simulated DFN by applying the moving window algorithm. Finally, we discuss the upscaled hydraulic conductivity fields and compare hydraulic heads at the fine- and coarse-scales.

3.5.1 Model configuration and parametrization at the fine-scale

We applied the methodology explained in subsection 3.2.2 to fit the theoretical pdf to the six datasets of fracture parameters. In this regard, we evaluate the goodness-of-fit of the theoretical pdfs via the Smirnov-Kolmogorov test with a degree of significance (α) of 0,05. Table 6. summarizes the most relevant results of such statistical modeling, according to the fractured family. The best fitted theoretical pdfs, for each parameter of interest, are the following: (i) the Fisher distribution for orientation (all families), (ii) the two-parameter Log-Normal distribution for spacing (all families), (iii) the negative exponential (families F1, F2, F3, F4, F5) and normal (family F6) distributions for persistence, and (iv) the one-parameter exponential distribution for opening (all families).

Table 6. Expected values of the pdf adjusted to the statistical distribution of the fractures' geometric variables that make up the different families of discontinuities.

Parameter fracture	F-1	F-2	F-3	F-4	F-5	F-5
Orientation (k-Fisher) (dimensionless)	9,46	9,82	14,31	13,27	20,91	27,91
Spacing (m)	0,31	0,36	0,31	0,32	0,33	0,35
Persistence (m)	1,81	1,05	0,98	0,84	1,08	1,10
Opening (mm)	3,07	3,65	3,99	3,55	2,67	1,90

Although Table 6. reports the expected values of the best fitted theoretical pdfs for all fracture families observed in the Dunita of Medellin geological unit, our upscaling experiment only

considers three of them, F3, F5, and F6. The selection of families is based on 2 aspects: First, we avoid saturating the fracture network with 6 families of discontinuities that do not necessarily occur at the same time in all mapped outcrops. Second, we selected 3 families that, when generating the fracture networks, allow us to obtain an anisotropic medium due to the strong changes in orientation between the fractures of different families and the hydraulic conductivity of each fracture.

Furthermore, to guarantee the occurrence of laminar flow within the fractures, we consider a fraction of the actual openings in the generation of the synthetic fractured media. Following this consideration, we adopt mean openings of 0,1 mm, 0,005 mm, and 0,02 mm for families F3, F5, and F6, respectively. With that, the cubic law is valid for estimating the fine-scale hydraulic conductivity of the fractures.

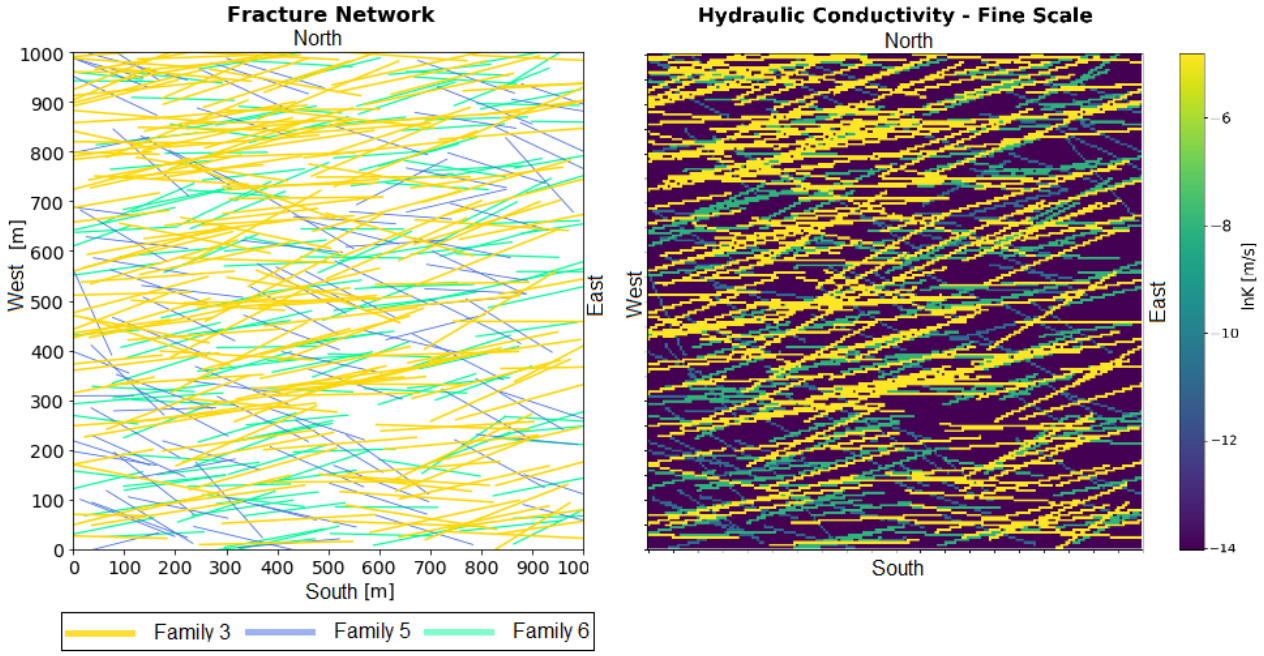

Figure 10. Representation of a fracture network for fracture families 3, 5, and 6 and hydraulic conductivity field in fine-scale. Own elaboration.

Figure 10 (map on the left) presents the modeling domain, which has an area of 1 km^2 (1 km x 1 Km). The thickness of the modeling area is one. For such an area, we generated a DFN using the theoretical pdfs fitted for the fracture parameters of families F3, F5, and F6. Figure 10 (map on the right) presents the hydraulic conductivity field estimated for the simulated DFN by applying the cubic law to each fracture and the moving window algorithm. At the fine scale, all simulated fractures that belong to a particular family have the same hydraulic conductivity. Estimated fracture hydraulic conductivities have a variability of two orders of magnitude (8,15 x 10^{-3} m/s and 2,04 x

10^{-5} m/s), whereas the hydraulic conductivity of the rock matrix is 8,15 x 10^{-7} m/s (see conventions of the color palette of Figure 10, map on the right). Families F3 and F5 are the ones with the highest and lowest hydraulic capacity, respectively. We discretize the modeling area using a regular grid of 200 x 200 cells. The dimensions of each cell are 5 m x 5 m.

Figure 11 presents the prescribed hydraulic heads and no-flow condition configuration for the different scenarios of groundwater flow models. The same boundary conditions apply for models at the fine or the coarse scales. In this regard, we defined two different configurations of boundary conditions. In the first configuration (scenario 1), we generate a flow gradient from West to East by imposing heads of 10 m and 0 m in western and eastern borders, respectively. North and south borders are no-flow boundary conditions. For the second configuration (scenario 2), the hydraulic gradient is from south to north. In this case, we impose heads of 10 m and 0 m in the southern and northern borders, respectively. Western and Eastern borders configure no-flow boundary conditions, the hydraulic gradient in the preferential direction is 0.001.

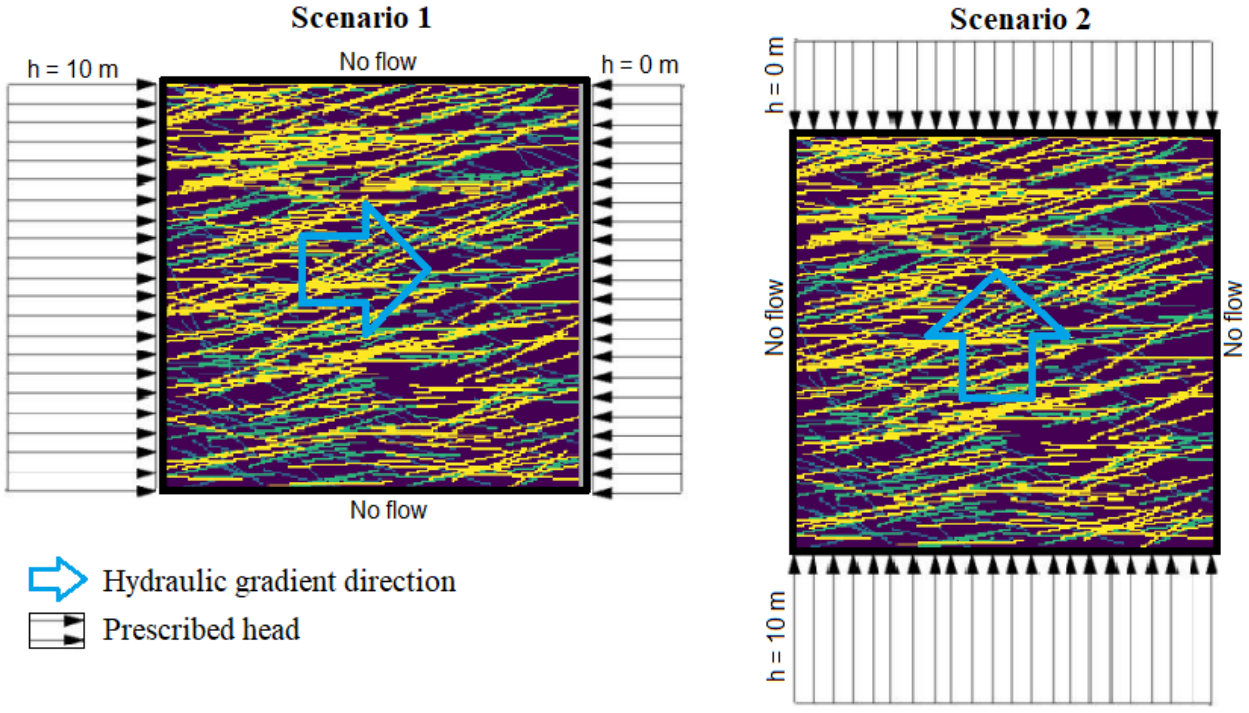

Figure 11. Prescribed hydraulic heads and no-flow condition location to evaluate groundwater flow models at the fine or the coarse scales.

3.5.2 Upscaled hydraulic conductivities and flows

We applied the Laplacian with skin upscaling method to the fine-scale hydraulic conductivity presented in Figure 10 (map on the right). The procedure considers the transformation of the

original fine-scale hydraulic conductivity field (cells of 5 m length) into two new upscaled fields with blocks of 10 m and 20 m length, respectively. Figure 12 shows the upscaled hydraulic conductivity fields as follows. Maps (A), (C), and (E) present the components K_{xx}, K_{yy}, and K_{xy} for the 10 m length upscaled hydraulic conductivity tensor. Maps (B), (D), and (F) present the components K_{xx}, K_{yy}, and K_{xy} for the 20 m length upscaled hydraulic conductivity tensor.

The upscaled fields show that the predominant component of the conductivity tensor is K_{xx} (see Figure 12 (A) and (B)) because the orientation of the most conductive fracture family (F3) is approximately from West to East. The magnitude of the K_{xx} component varies between 1 x 10^{-3} m/s and 8,15 x 10^{-7} m/s. Blocks with the high values of K_{xx} correspond to those collocated with the more conductive fracture families. The more West-East oriented is the fracture, the highest is the value of K_{xx} conversely, blocks with low values of K_{xx} correspond to those enclosing large areas of the rock matrix.

The upscaled fields for the K_{yy} component (see Figure 12C and D) indicate a low influence of the component (compared to K_{xx}) on groundwater flow through the fractured medium, due to the fractures' low hydraulic capacity close to the Northeast and Southwest directions. The magnitude of the K_{yy} component in the upscaled fields varies between 1.30 x 10^{-3} m/s and 8.15 x 10^{-7} m/s. At least 50% of the blocks in both meshes have a hydraulic conductivity with the same order of magnitude as the hydraulic conductivity of the rock matrix.

The upscaled magnitudes of the K_{xy} component of the hydraulic conductivity tensor (see Figure 12E and F) vary between 1.24 x 10^{-4} m/s and 8.31 x 10^{-8} m/s. Blocks with high hydraulic conductivities are located near fractures of families F3 and F6, which are the most conductive. Their orientation generates flows to the East by applying hydraulic gradients pointing to the North. Similarly to the K_{xx} component, blocks with values of K_{yy} close to the rock matrix hydraulic conductivity are in sectors where the fine-scale DFN have low fracture density.

We simulated groundwater flow dynamics using the fine-scale and the upscaled conductivity fields (see map on the right in Figure 10 and upscaled fields in Figure 12). Figure 13 shows the simulated hydraulic head fields as follows. Maps (A), (B), and (C) presents simulated hydraulic heads for scenario 1 (preferential flow from West to East) at the fine scale, 10 m block length, and 20 m block length, respectively. Similarly, maps (D), (E), and (F) illustrate simulated hydraulic heads for scenario 2 (preferential flow from South to North) at the fine scale, 10 m block length, and 20 m block length, respectively.

At the fine-scale (see Figure 13A and D), the existence of highly conductive fractures strongly influences the hydraulic heads' spatial variability. This effect is most evident in the simulations for scenario 1, for which the orientation of the fractures is similar to the main flow direction. The presence of discontinuities in the rock generates high hydraulic gradients, particularly in areas where the fracture density is high.

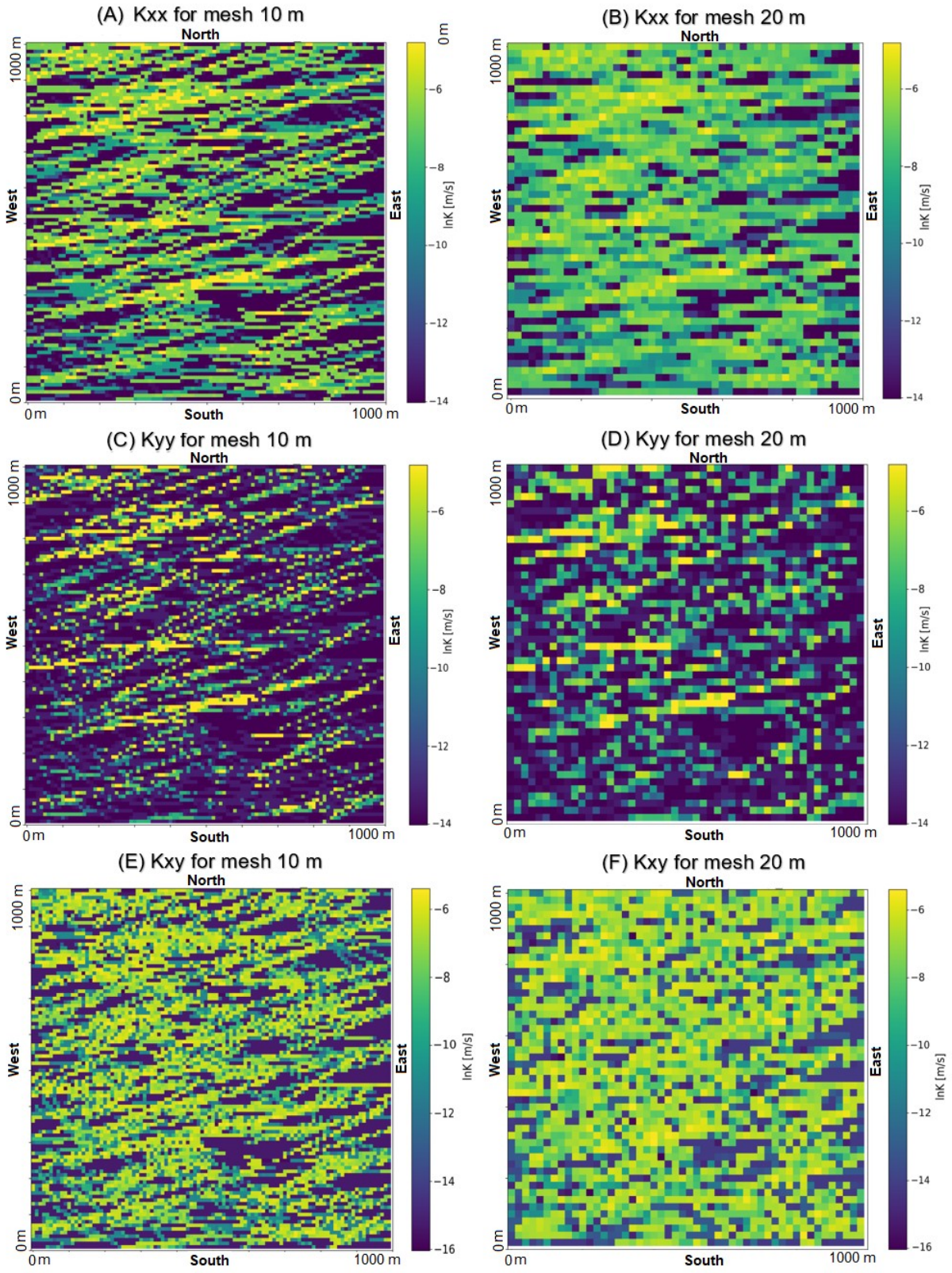

Figure 12. Spatial distribution of the upscaled K_{xx}, K_{yy} and K_{xy} components. Own elaboration

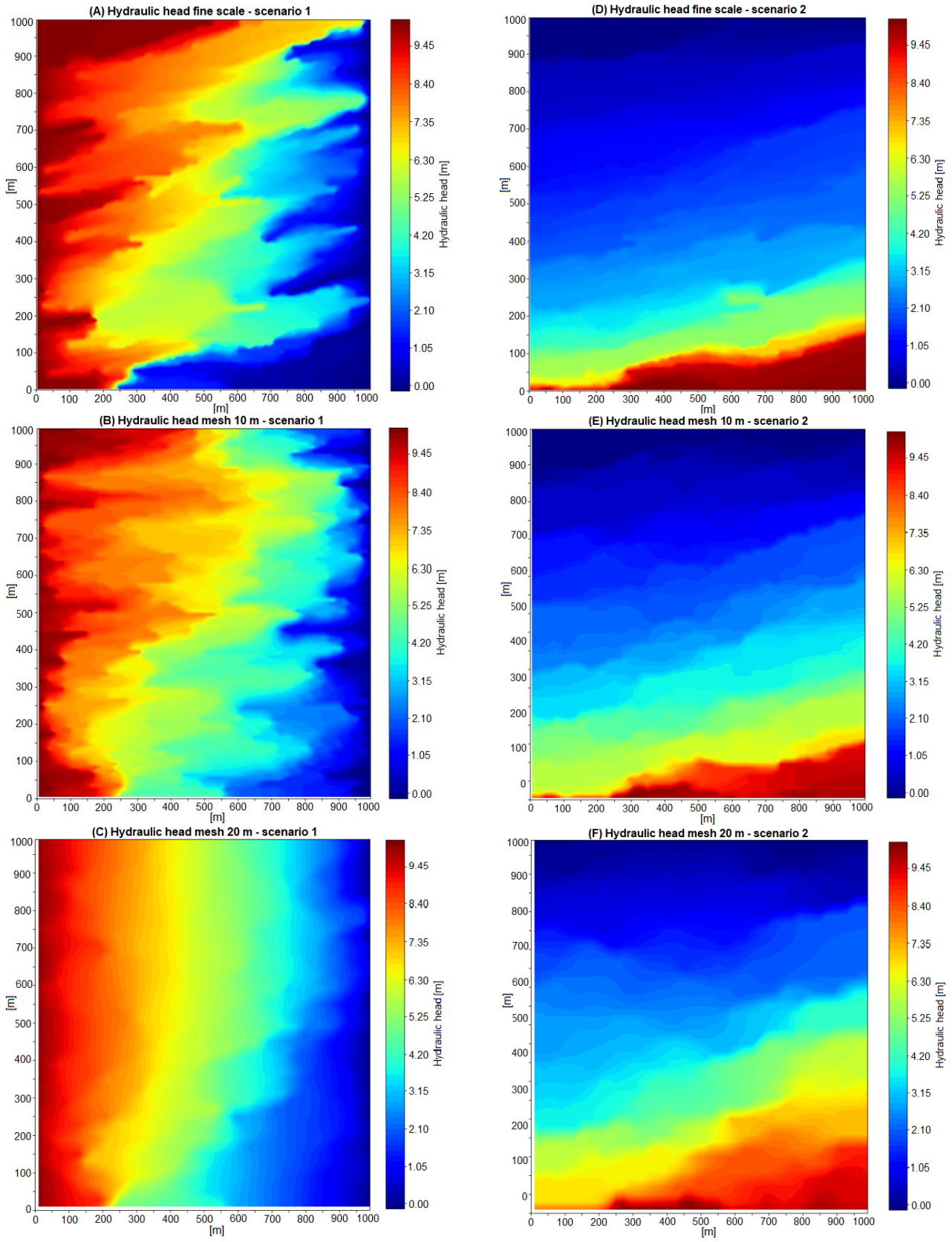

Figure 13. Simulated hydraulic heads at the fine and block scale. Own elaboration

Such gradients produce distinctive flow patterns that follow the orientation of the fractures. In particular, fracture family F3 controls the local flows along the direction N75E. Conversely, hydraulic head fields simulated for scenario 2 lack recognizable local flow patterns, but the rock fractures generate that the equipotential lines follow the direction N75E predominantly. Again, this feature illustrates that family F3 is the most critical hydraulic control of the local flow patterns.

Figure 13 presents the simulated heads for the hydraulic conductivities upscaled to a 10 m and 20 m length blocks. In scenario 1 (Figure 13B), although the main flow direction is preserved, the upscaling procedure smooths the simulated equipotential lines regarding the fine-scale simulation. Furthermore, some of the recognizable local flow patterns at the fine-scale disappeared or changed their aspect. For example, it is not possible to detect some of the areas on which the local flow patterns match the conductive fracture families' orientation. In other areas, although the local flow patterns at the fine-scale still exist, their spatial persistence is shorter. Hydraulic head fields simulated for scenario 2 (see Figure 13E) preserve most of the main patterns of variability observed at the fine-scale. Although it is not a general feature, upscaling the hydraulic conductivity fields removed some recognizable local flow patterns, most of them occurring in transition areas (from high to low heads).

As the upscaling procedure acts in larger areas, the heterogeneity of the hydraulic conductivity fields reduces. At the same time, the simulated heads do not show the variability observed at the fine-scale. In this regard, Figure 13 presents the simulated hydraulic heads at the scale of 20 m block size (see maps (C) and (F) for scenarios 1 and 2, respectively). The simulated hydraulic head fields are smoother because many fracture connectivity artifacts appear in the upscaled conductivity fields. For scenario 1, all the fine-scale local flow patterns vanish as the effect of upscaling. For scenario 2, areas on which simulated heads are higher than 7 m are more extensive than those observed at the fine-scale. These results imply: (i) essential modifications in the local groundwater flow dynamics regarding the fine-scale observations, (ii) a decrease in representativeness and reliability of the upscaled models, and (iii) the existence of a block size threshold on which the upscaled hydraulic conductivities no longer represent the fine-scale variability accurately. In the following, we estimate performance metrics to quantify the limits of representativeness of the upscaled models.

Figure 14 presents scatter plots and residual histograms for comparing the fine-scale hydraulic heads with the upscaled ones. The graphics (A) and (C) present the results for scenario 1 at the 10 m and 20 m block length scale, respectively. Similarly, the graphics (B) and (D) show the results for scenario 2. The scatterplot in graphics (A) and (B) show that the respective point clouds (fine-

scale head versus 10 m scale head) distribute along the unitary slope line, which means an accurate reproduction of the fine-scale heads. Although this observation is valid for scenarios 1 and 2, the point cloud of scenario 2 is narrower than the one for scenario 1. Estimates of RMSE provide us a quantification of the representativeness of the upscaled heads. At the 10 m scale, we estimate RMSE of 0.86 m and 0.52 m for scenarios 1 and 2, respectively. Since the point cloud of scenario 1 is vast, the upscaled hydraulic conductivity field causes considerable under and overestimations of the small-scale heads. On the other hand, since the point cloud of scenario 2 is narrow, the magnitude of the upscaling errors is relatively small.

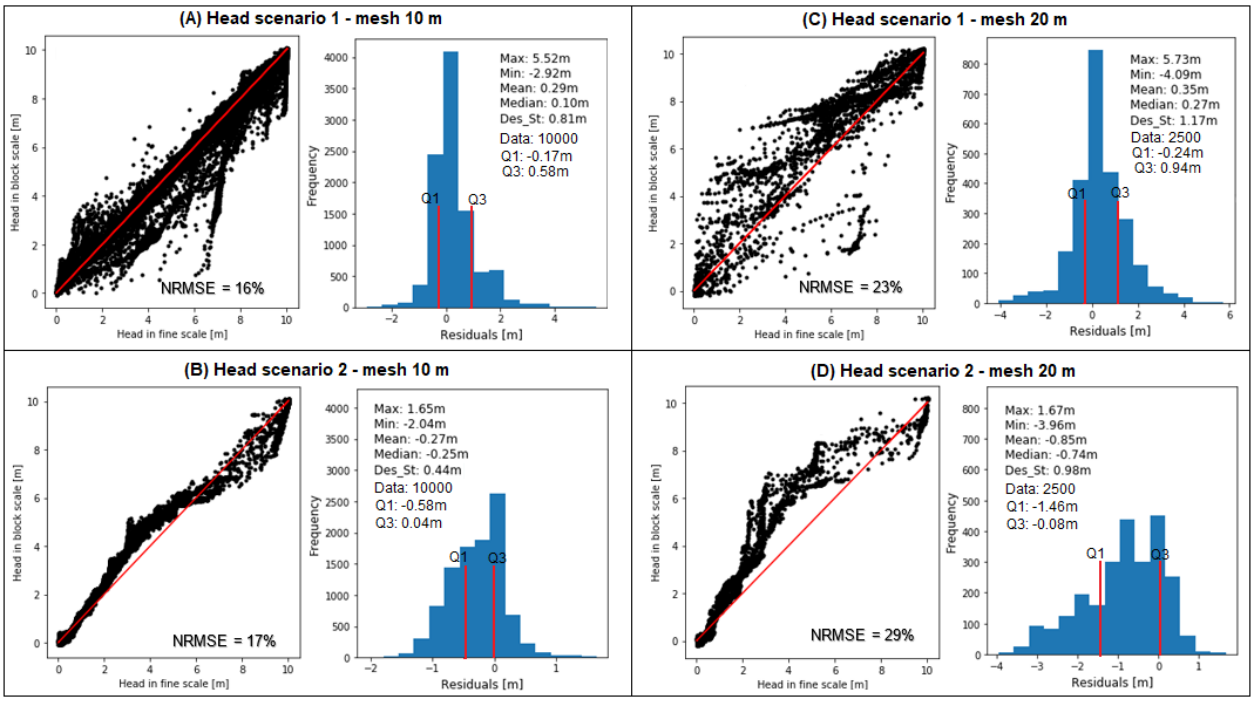

Figure 14. Comparison of hydraulic heads between fine scale and block scale for hydraulic conductivity fields made up of square blocks of 2 and 4 size. The red line (unit line) represents the zero difference between the hydraulic loads of the fine scale and the block scale. Own elaboration

Histograms in graphics (A) and (B) summarizes the statistical behavior of the upscaled head residuals (fine-scale head versus 10 m scale head). Red lines mark the location of the quartiles of the residual pdf. The mean and median residual estimated for scenario 1 are 0.29 m and 0.10 m, respectively, which means that the upscaling procedure compensates for the errors. Despite the above, the maximum and minimum residuals are 5.52 m and -2.92 m, respectively. The range of the residuals explains the wideness of the point cloud in the head scatterplot. The most remarkable characteristics of the head residuals computed for the upscaling in scenario 2 are the following: (i) the mean and median are -0.27 m and -0.25 m, respectively, (ii) the minimum and maximum are -2.04 m and 1.65 m, respectively, (iii) the standard deviation is 0.44 m, and (iv) the

interquartile range is 0.54 m. These estimates show that the flows upscaled for scenario 2 are more accurate than the ones scaled for scenario 1.

For hydraulic heads in the mesh with blocks of 20 m length, scatterplots in graphics (C) and (D) show that the respective point clouds (fine-scale head versus 20 m scale head) distribute following the trend of the unit slope line, but with greater dispersion than the point cloud obtained for a 10 m scale head. This represents a deterioration in the reproduction of fine-scale heads in the coarse-scale when the size of the superblocks in the mesh is increased. Like the simulated heads in the 10 m mesh, in the mesh with blocks of 20 m length, the point cloud of scenario 2 is narrower than scenario 1. However, the mean (0.35 m) and median (0.27 m) of the residuals of scenario 1 are lower than the mean (-0.85m) and median (-0.74 m) of the residuals of scenario 2. Estimates of RMSE provide us a quantification of the representativeness of the upscaled heads. At the 20 m scale, we estimate RMSE of 1.20 m and 1.30 m for scenarios 1 and 2, respectively. Both errors are appreciable if it is taken into account that they represent deviations of 23% and 29%, with respect to the average of the heads on the fine-scale for scenarios 1 and 2, respectively. The errors that we calculate for the heads of scenarios 1 and 2 in the scaled medium with a 20 m mesh are 7 and 12 percentage points above the errors we obtained when evaluating both scenarios in the scaled medium with a 10 m mesh, respectively.

Histograms in graphics (C) and (D) summarize the statistical behavior of the upscaled head residuals (fine-scale head versus 20 m scale head). Red lines mark the location of the quartiles of the residual distribution. For the mesh with blocks of 20 m, the errors of the calculation of the heads are not compensated. The histograms of the residuals show biases, causing the errors' mean value to move away from zero. In scenario 1, the biases are underestimated, i.e.piezometric levels lower than those observed in the fine-scale are estimated, while in scenario 2, there are overestimations. This behavior is typical of a smoothing in the fields of hydraulic conductivity. They mean that scaling reduces much of the hydraulic conductivity variability within the block; i.e., it eliminates local effects caused by fracturing.

The most remarkable characteristics of the head residuals computed for the upscaling in scenario 2 are the following: (i) the mean and median are -0.85 m and -0.74 m, respectively, (ii) the minimum and maximum are -3.96 m and 1.67 m, respectively, (iii) the standard deviation is 0.98 m, and (iv) the interquartile range is 1.38 m. These estimates show that the flows upscaled for scenario 1 are more accurate than those scaled for scenario 2 in the mesh with 20 m length blocks.

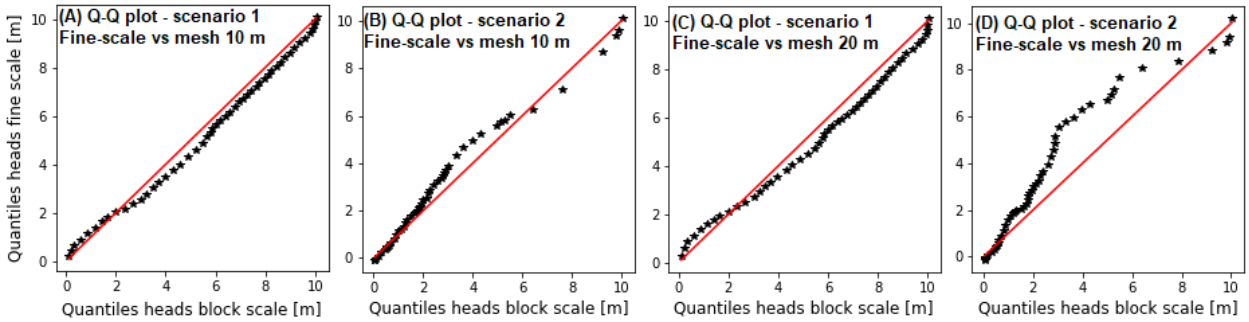

Figure 15. Comparison of quantiles of simulated hydraulic heads in the fine and block scales.

Figure 15 presents $Q-Q$ plots of the upscaled head empirical pdfs versus the fine-scale pdf. If the two pdf are similar, the estimated pair of percentiles lies on the line $Q_{fine} = Q_{upscaled}$, where Q_{fine} is the i[th] percentile of the fine-scale pdf and $Q_{upscaled}$ is the i[th] percentile of upscaled pdf. Labels from (A) to (D) denote the results for scenarios 1 and 2 and the corresponding modeling scales (10 m and 20 m block size). $Q-Q$ plots estimated for heads at the scale of 10 m block size versus the fine-scale heads follows approximately the unitary slope line (see plots (A) and (B)). This result allows us to conclude that hydraulic conductivity fields at the 10 m scale reproduce most of the fine-scale variability patterns. The corresponding pdfs of the simulated heads are also representative. However, head percentiles estimated for scenario 1 exhibit a recurrent overestimation of 0.4 m, while percentiles estimated for scenario 2 show a considerable underestimation in the range [2.0 m, 4.0 m].

$Q-Q$ plots estimated for heads at the scale of 20 m block size versus the fine-scale heads follows approximately the unitary slope line (see plots (C) and (D)). In this scale, the estimated head percentiles for scenario 1 continue to show an overestimation, and in the case of scenario 2, an underestimation in the range of [2.0 m, 7.0 m]. The differences between the percentiles of both scenarios are exaggerated with respect to the simulated heads at a 10 m block scale. This result allows us to conclude that the hydraulic conductivity fields in the scale of blocks of 20 m length reproduce with less precision (compared to the scale blocks of 10 m) the patterns of variability of the heads observed in the fine-scale, mainly for scenario 2. Such discrepancy between the heads of the different scales is due to the simplification made when representing the variability of the fractures' hydraulic conductivity in the components of the hydraulic conductivity tensor scaled.

3.5.3 Improvement of the computational efficiency

To evaluate the reduction in computational requirements due to scaled hydraulic conductivity models, we determined the execution time and memory space occupied by the flow models

evaluated in the fine and block scale. Table 7. shows the time and memory space calculated for the three models and the reduction of both requirements in the scaled models with respect to the fine-scale model. Models run in the upscaled hydraulic conductivity fields show that a scaling step reduces by at least 90% the runtime and memory storage required by the model in the fine-scale. The improvement in the evaluation of the model is due to the reduction of the size of the matrix of coefficients used in resolving the groundwater flow model.

The reduction in computational requirements of our hydraulic conductivity scaling exercises, compared to the fine-scale models, was determined in steady-state flow models. We consider that the scaled models' performance can significantly improve the realization of groundwater flow models in fractured media, given the reduction in the computation times of the transient models and the memory storage required by the runs.

Table 7. Comparison of time and storage space required in memory during the execution of the fine-scale and block-scale models. Own elaboration

Model	Time (seg)	Size matrix (Mb)	Reduction time (%)	Reduction size matrix (%)
200x200 (reference)	128	12800	-	-
100x100	2,80	800	97,81%	93,75%
50x50	0,43	50	99,66%	99,60%

3.6 Conclusions

In this work, we investigate the possibilities of using the Laplacian-with-skin method to scale a fractured medium's hydraulic conductivity. Our computational experiments consider different configurations of boundary conditions and a highly heterogeneous medium of hydraulic conductivities due to fracture networks, which impact the scaling method's precision. Although our results show that scaling with small blocks does not seriously impact the representativeness of fine-scale flow processes, for coarse scales with large blocks, precision is lost in the representation of the variability of heads observed at a fine scale. The degree of precision lost due to the scaling effect depends on the relative configuration between the preferential flow direction and fracture networks' characteristics. In particular, increasing the coarse-scale from 10 m blocks to 20 m blocks considerably reduces the heterogeneity (homogenization) of the hydraulic conductivity field observed on the fine-scale. Homogenization of hydraulic conductivities occurs due to the appearance of connectivity between fractures within the coarse-scale blocks, which is not necessarily true in the original fracture network.

For the piezometric heights evaluated in the scaled medium with a 10 m mesh, some of the flow patterns observed in the fine-scale are preserved. Such patterns are controlled by the fractures' orientation and the hydraulic gradient generated on the fine-scale in sectors with high contrast hydraulic conductivity (the difference between the rock matrix's hydraulic conductivity and the conductivity of the fracture). In the scaled field with the 20 m mesh, the blocks enclose large areas with a significant hydraulic conductivity of the rock matrix and fractures, causing the resulting of equivalent tensors to present significantly less variability than the variability of the hydraulic conductivity observed in the fine-scale. This result shows that the block's size represents the major limitation in the Laplacian-with-skin method's applicability to simulate groundwater flow in fractured media using equivalent porous media.

The hydraulic conductivity fields scaled with blocks of 10 m in length compensate for the errors obtained in calculating the piezometric levels. Such is not the case for hydraulic conductivity fields scaled with blocks of 20 m length. The 20 m blocks scale areas four times greater than the 10 m blocks, strongly impacting the heterogeneity's hydraulic conductivity fields by eliminating local effects caused by fractures. The loss of the fine scale's flow patterns is due to two effects of scaling in the fractured medium. The first effect of scaling is the elimination of strong local hydraulic conductivity contrasts caused by fractures. The second effect is the reduction of hydraulic gradients in scaled fields due to these fields' smoothness, especially in fields with 20 m blocks.

If hydraulic conductivity tensors with suitable block sizes can be determined, then the scaled conductivity fields with the Laplacian-with-skin method could be used in regional studies. The advantage of the above is that the computational load in the execution of flow models is considerably reduced. In contrast, the main characteristics of the variability of the fine-scale flow are adequately represented. However, a preliminary sensitivity analysis should be done to determine a block size for scaling that does not dramatically reduce the spatial variability of fine-scale hydraulic conductivity and, consequently, the most critical regional flow patterns.

We have found that block scale results for hydraulic heads improve when fracture families are adequately represented in the field of hydraulic conductivity. By the adequate representation of fractures in the conductivity field, we mean using a mobile window whose size encloses fractures from the same family.

The best correlation between the hydraulic heads simulated on the fine-scale and those simulated on the block scale was obtained for the scaled fields using a skin size equal to or greater than

50% of the block size. This condition coincides with the scaling of a porous medium made by Gómez-Hernández (1991).

Our methodology promises a considerable improvement in the performance of the flow models evaluated in finely discretized fractured media. However, for its efficient use in real management models, our methodology requires optimizing some processes executed during escalation. Our results show that the preferential flow direction, together with the fracture network's orientation, influences the quality of the scaled models. The above makes it necessary to consider the fact that the flow models resulting from scaling can show essential modifications in the dynamics of the local groundwater flow with respect to fine-scale observations. Hence the importance of determining suitable block sizes for the coarse-scale and being able to compensate for acceptable losses in flow representation with the good computational performance associated with scaled conductivity fields.

4 Global Conclusions

The scaling methodology that we have implemented in this research represents a contribution in the modeling the fractured medium with a continuous approach. Our methodology estimates the equivalent hydraulic conductivity tensor based on fracture networks' geometric and hydraulic properties. Also, it reliably reproduces the flow characteristics in the fractured medium observed on the fine-scale.

We have approached the representation of fractured media in large scale flow models, using equivalent hydraulic conductivity tensors representing the variability of fracture networks in coarse scale blocks. Hydraulic conductivity fields scaled with the Laplacian-with-skin method notably redeem the variability of hydraulic conductivity in large blocks. However, if suitable block sizes are defined through sensitivity analysis before model evaluation, scaled conductivity fields can be obtained to represent flow dynamics accurately.

Our flow models evaluated in a coarse-scale show that the Laplacian-with-skin method can generate scaled hydraulic conductivity fields capable of accurately representing flow in a fractured medium, as long as block sizes are used that do not significantly smooth the variability of the fine-scale hydraulic conductivity. Scaling generates flow models with computational requirements substantially lower than those achieved in fine-scale models. Therefore, the scaled fields of hydraulic conductivity represent an improvement in flow models' performance in fractured media on large scales.

5 Bibliography

Ababou, R., Millard, A., Treille, E., Durin, M., & Plas, F. (1994). Continuum Modeling of Coupled Thermo-Hydro-Mechanical Processes in Fractured Rock. *Computational Methods in Water Resources X*, *3*(2), 651–658. https://doi.org/10.1007/978-94-010-9204-3_79

Anderson, M. P., Woessner, W. W., & Hunt, R. J. (2015). *Applied Groundwater Modeling: Simulation of Flow and Advective Transport* (Second). ELSEVIER.

Ando, K., Kostner, A., & Neuman, S. P. (2003). Stochastic continuum modeling of flow and transport in a crystalline rock mass: Fanay-Augères, France, revisited. *Hydrogeology Journal*, *11*(5), 521–535. https://doi.org/10.1007/s10040-003-0286-0

Assteerawatt, A. (2008). Flow and Transport Modelling of Fractured Aquifers based on a Geostatistical Approach. In *Transport*. https://doi.org/10.1097/MOT.0000000000000119

Bear, J. (1972). *Dynamics of Fluids in Porous Media* (Dover Publication (ed.)).

Bear, J., & Cheng, A. H.-D. (2010). Water Balance and Complete Flow Model. In *Modeling Groundwater Flow and Contaminant Transport* (p. 815). https://doi.org/10.1007/978-1-4020-6682-5

Bear, J., Tsang, C.-F., & Marsily, G. De. (1993). *Flow and Contaminant Transport in Fractured Rock*. https://books.google.com/books?id=7UIqLGoJMjcC&pgis=1

Begg, S. H., Carter, R. R., & Dranfield, P. (1989). Assigning Effective Values to Simulator Gridblock Parameters for Heterogeneous Reservoirs. *SPE Reservoir Engineering*, *4*(04), 455–463. https://doi.org/10.2118/16754-PA

Begg, S. H., & King, P. R. (1985). Modelling the Effects of Shales on Reservoir Performance: Calculation of Effective Vertical Permeability. *SPE Reservoir Simulation Symposium*, 1–16. https://doi.org/10.2118/13529-MS

Beran, M. J., & Pytte, A. (1968). Statistical Continuum Theories. *American Journal of Physics*, *36*(10), 923–923. https://doi.org/10.1119/1.1974326

Berkowitz, B. (2002). Characterizing Flow and Transport in Fractured Geological Media: A Review. *Advances in Water Resources*, *25*(8–12), 861–884. https://doi.org/10.1016/S0309-1708(02)00042-8

Berkowitz, B., Bear, J., & Braester, C. (1988). Continuum Models for Contaminant Transport in Fractured Porous Formations. *Water Resources Research*, *24*(8), 1225–1236. https://doi.org/10.1029/WR024i008p01225

Blöschl, G., & Sivapalan, M. (1995). Scale Issues in Hydrological Modelling: A Review. *Hydrological Processes*, *9*(3–4), 251–290. https://doi.org/10.1002/hyp.3360090305

Botros, F., Hassan, A., & Pohll, G. (2006). Assessment of Hydraulic Conductivity Upscaling Techniques and Associated Uncertainty. *XVI International Conference on Computational Methods in Water Resources*, 1–8. https://doi.org/10.4122/1.1000000475

Bouwer, H. (1969). Planning and Interpreting Soil Permeability Measurements. *Journal of Irrigation and Drainage Engineering*, *95*(3), 391–402.

Cacas, M. C., Ledoux, E., de Marsily, G., Tillie, B., Barbreau, A., Durand, E., Feuga, B., & Peaudecerf, P. (1990). Modeling Fracture Flow with a Stochastic Discrete Fracture Network: Calibration and Validation: 1. The Flow Model. *Water Resources Research*, *26*(3), 479–489. https://doi.org/10.1029/WR026i003p00479

Cardwell, W. T., & Parsons, R. L. (1945). Average Permeabilities of Heterogeneous Oil Sands. *Transactions of the AIME*, *160*(01), 34–42. https://doi.org/10.2118/945034-G

Chen, M., Bai, M., & Roegiers, J. C. (1999). Permeability Tensors of Anisotropic Fracture Networks. *Mathematical Geology*, *31*(4), 355–373. https://doi.org/10.1023/A:1007534523363

Cook, P. G., Land, C., & Osmond, G. (2003). A Guide To Regional Flow In Fractured Rock Aquifers. In *Water*. http://lwa.gov.au/files/products/river-landscapes/px020312/px020312.pdf

Cvetkovic, V., Painter, S., Outters, N., & Selroos, J. O. (2004). Stochastic simulation of radionuclide migration in discretely fractured rock near the Äspö Hard Rock Laboratory. *Water Resources Research*, *40*(2). https://doi.org/10.1029/2003WR002655

Dagan, G. (1979). Models of Groundwater Flow in Statistically Homogeneous Porous Formations. *Water Resources Research*, *15*(1), 47–63. https://doi.org/10.1029/WR015i001p00047

Dagan, G. (1981). Analysis of Flow Through Heterogeneous Random Aquifers by the Method of Embedding Matrix. 1. Steady Flow. *Water Resources Research*, *18*(5), 107–121. https://doi.org/10.1029/WR017i001p00107

De Wit, A. (1995). Correlation Structure Dependence of the Effective Permeability of Heterogeneous Porous Media. *Physics of Fluids*, *7*(11), 2553–2562. https://doi.org/10.1063/1.868705

Dershowitz, W., Wallmann, P., & Kindred, S. (1991). *Discrete fracture modelling for the Stripa site characterization and validation drift inflow predictions. Stripa Project Tech Rep 91–16* (Issue June). https://inis.iaea.org/search/search.aspx?orig_q=RN:23030434

Durlofsky, L. J. (1991). Numerical Calculation of Equivalent Grid Block Permeability Tnesors for Heterogeneous Porous Media. *Water Resources Research*, *27*(5), 699–708. https://doi.org/10.1029/91wr00107

Durlofsky, L. J. (1992). Representation of grid block permeability in coarse scale models of randomly heterogeneous porous media. *Water Resources Research*, *28*(7), 1791–1800. https://doi.org/10.1029/92WR00541

Emanuel, A. S., Alameda, G. K., Behrens, R. A., & Hewett, T. A. (1989). Reservoir performance prediction methods based on fractal geostatics. *SPE Reservoir Engineering (Society of Petroleum Engineers)*, *4*(3). https://doi.org/10.2118/16971-pa

Fadakar Alghalandis, Y. (2017). ADFNE: Open Source Software for Discrete Fracture

Network Engineering, Two and Three Dimensional Applications. *Computers and Geosciences*, *102*, 1–11. https://doi.org/10.1016/j.cageo.2017.02.002

Fisher, R. (1953). Dispersion on a Sphere. *Proceedings of the Royal Society A: Mathematical, Physical and Engineering Sciences*, *217*(1130), 295–305. https://doi.org/10.1098/rspa.1953.0064

Freeze, R.A., Cherry, J. A. (1979). *Groundwater* (B. Cathy & K. McNeily (eds.)). Prentice-Hall. http://hydrogeologistswithoutborders.org/wordpress/

Fu, J., Axness, C. L., & Gomez-Hernandez, J. J. (2011). Upscaling transmissivity in the near-well region for numerical simulation: A comparison on uncertainty propagation. *Engineering Applications of Computational Fluid Mechanics*, *5*(1), 49–66. https://doi.org/10.1080/19942060.2011.11015352

Ghasemizadeh, R., Yu, X., Butscher, C., Hellweger, F., Padilla, I., Alshawabkeh, A., & Cao, B. Y. (2015). Equivalent porous media (EPM) simulation of groundwater hydraulics and contaminant transport in Karst aquifers. *PLoS ONE*, *10*(9), 1–21. https://doi.org/10.1371/journal.pone.0138954

Gómez-Hernández, J. (1991). A Stochastic Approach to the Simulation of Block Conductivity Fields Conditioned Upon Data Measured at a Smaller Scale. In *Sciences-New York*. Stanford University.

Gupta, V. K., Rodriguez-Iturbe, I., & Wood, E. F. (1986). *Scale Problems in Hydrology* (V. K. Gupta, I. Rodriguez-Iturbe, & E. F. Wood (eds.); 1st ed.). Springer Netherlands. https://doi.org/10.1007/978-94-009-4678-1

Hadgu, T., Karra, S., Kalinina, E., Makedonska, N., Hyman, J. D., Klise, K., Viswanathan, H. S., & Wang, Y. (2017). A comparative study of discrete fracture network and equivalent continuum models for simulating flow and transport in the far field of a hypothetical nuclear waste repository in crystalline host rock. *Journal of Hydrology*, *553*, 59–70. https://doi.org/10.1016/j.jhydrol.2017.07.046

Hassan, A. E., Bekhit, H. M., & Chapman, J. B. (2008). Uncertainty assessment of a stochastic groundwater flow model using GLUE analysis. *Journal of Hydrology*,

362(1–2), 89–109. https://doi.org/10.1016/j.jhydrol.2008.08.017

Herbert, A., Gale, J., Lanyon, G., & MacLeod, R. (1991). *Modelling For the Stripa Site Characterization and Validation Drift Inflow: Prediction of Row Through Fractured Rock. Stripa Project Tech Rep 91–35* (Issue December). https://inis.iaea.org/search/search.aspx?orig_q=RN:23071050

Hewett, T. A., & Behrens, R. A. (1993). Considerations affecting the scaling of displacements in heterogeneous permeability distributions. *SPE Formation Evaluation*, *8*(4), 258–266. https://doi.org/10.2118/20739-PA

Huang, N., Jiang, Y., Li, B., & Liu, R. (2016). A numerical method for simulating fluid flow through 3-D fracture networks. *Journal of Natural Gas Science and Engineering*, *33*, 1271–1281. https://doi.org/10.1016/j.jngse.2016.06.072

Indelman, P. (1996). Averaging of unsteady flows in heterogeneous media of stationary conductivity. *Journal of Fluid Mechanics*, *310*, 39–60. https://doi.org/10.1017/S0022112096001723

Indelman, P., & Dagan, G. (1993). Upscaling of Permeability of Anisotropic Heterogeneous Formations: 1. The General Framework. *Water Resources Research*, *29*(4), 935–943. https://doi.org/10.1029/92WR02448

Jing, L., & Stephansson, O. (2007). Discrete Fracture Network (DFN) Method. Developments in Geotechnical Engineering. In L. Jing & O. Stephansson (Eds.), *Fundamentals of Discrete Element Methods for Rock Engineering* (pp. 365–398). https://doi.org/10.1016/S0165-1250(07)85010-3

Journel, A. G., Deutsch, C., & Desbarats, A. J. (1986). Power Averaging for Block Effective Permeability. In *SPE California Regional Meeting* (p. 6). Society of Petroleum Engineers. https://doi.org/10.2118/15128-MS

King, P. R. (1989). The use of renormalization for calculating effective permeability. *Transport in Porous Media*, *4*(1), 37–58. https://doi.org/10.1007/BF00134741

Kiraly, L. (1969). Anisotropie et hétérogénéité de la perméabilité dans les calcaries fissurés. *Eclogae Geologicae Helvetiae*, *62*(2), 613–619.

http://doc.rero.ch/record/259382/files/Kiraly_L._-_Anisotropie_et_h_t_rog_n_it_de_la_perm_abilit_ETH_EGH_62_1969.pdf

Klepikova, M. V., Le Borgne, T., Bour, O., & Davy, P. (2011). A methodology for using borehole temperature-depth profiles under ambient, single and cross-borehole pumping conditions to estimate fracture hydraulic properties. *Journal of Hydrology*, *407*(1–4), 145–152. https://doi.org/10.1016/j.jhydrol.2011.07.018

Klimczak, C., Schultz, R. A., Parashar, R., & Reeves, D. M. (2010). Cubic law with aperture-length correlation: implications for network scale fluid flow. *Hydrogeology Journal*, *18*(4), 851–862. https://doi.org/10.1007/s10040-009-0572-6

Kulatilake, P. H. S. W., Fellow, ASCE, & Panda, B. B. (2000). Effect of block size and joint geometry on jointed rock hydraulics and REV. *Journal of Engineering Mechanics*, *August*, 850–858.

Langevin, C. D., Hughes, J. D., Banta, E. R., Niswonger, R. G., Panday, S., & Provost, A. M. (2017). Documentation for the MODFLOW 6 Groundwater Flow Model: U.S. Geological Survey Techniques and Methods. In *Book 6, Modeling Techniques* (p. 197). U.S. Geological Survey. https://pubs.usgs.gov/tm/06/a55/tm6a55.pdf

Lavenue, M., & Marsily, G. de. (2001). Three-dimensional interference test interpretation in a fractured aquifer using the pilot point inverse method Marsh. *Water Resources Research*, *37*(11), 2659–2675. https://doi.org/10.1029/2000WR000289

Lei, Q., Latham, J. P., & Tsang, C. F. (2017). The use of discrete fracture networks for modelling coupled geomechanical and hydrological behaviour of fractured rocks. *Computers and Geotechnics*, *85*, 151–176. https://doi.org/10.1016/j.compgeo.2016.12.024

Li, L., Zhou, H., & Gómez-Hernández J. Jaime, J. (2011a). Transport upscaling using multi-rate mass transfer in three-dimensional highly heterogeneous porous media. *Advances in Water Resources*, *34*(4), 478–489. https://doi.org/10.1016/j.advwatres.2011.01.001

Li, L., Zhou, H., & Gómez-Hernández J. Jaime, J. J. (2011b). A comparative study of

three-dimensional hydraulic conductivity upscaling at the macro-dispersion experiment (MADE) site, Columbus Air Force Base, Mississippi (USA). *Journal of Hydrology*, *404*(3–4), 278–293. https://doi.org/10.1016/j.jhydrol.2011.05.001

Li, L., Zhou, H., Hendricks Franssen, H. J., & Gómez-Hernndez, J. J. (2012). Modeling transient groundwater flow by coupling ensemble Kalman filtering and upscaling. *Water Resources Research*, *48*(1). https://doi.org/10.1029/2010WR010214

Li, L., Zhou, H., & Jaime Gómez-Hernández, J. (2010). Steady-state saturated groundwater flow modeling with full tensor conductivities using finite differences. *Computers and Geosciences*, *36*(10), 1211–1223. https://doi.org/10.1016/j.cageo.2010.04.002

Llerar-Meza, G. (2009). *Upscaling non-reactive solute transport*. Universidad Politécnica de Valencia.

Loc'H, G. Le. (1987). *Étude de la composition des perméabilités par des méthodes variationelles*. [S.n].

Londoño Aguirre, R. D. (2015). *Definición de un Volumen Elemental de Referencia y Estimación de un Modelo de Conductividades Hidráulicas Equivalentes para un Sistema Acuífero en un Medio Fracturado* [Universidad Nacional de Colombia - Medellín]. http://www.bdigital.unal.edu.co/50039/2/1128448123.2015-2.pdf

Long, J. C. S., Remer, J. S., Wilson, C. R., & Witherspoon, P. A. (1982). Porous media equivalents for networks of discontinuous fractures. *Water Resources Research*, *18*(3), 645–658. https://doi.org/10.1029/WR018i003p00645

Maréchal, J. C., Dewandel, B., & Subrahmanyam, K. (2007). 7. Characterization of fracture properties in hard rock aquifer system. In *Groundwater* (pp. 156–188). https://doi.org/10.1007/978-1-4020-5729-8_7

Martinez-Landa, L., & Carrera, J. (2006). A methodology to interpret cross-hole tests in a granite block. *Journal of Hydrology*, *325*(1–4), 222–240. https://doi.org/10.1016/j.jhydrol.2005.10.017

Matheron, G. (1967). *Élèments pour une théorie des milieux poreux* (p. 168 p.). Masson

et Cie. file://catalog.hathitrust.org/Record/000724901

Min, K. B., Jing, L., & Stephansson, O. (2004). Determining the equivalent permeability tensor for fractured rock masses using a stochastic REV approach: Method and application to the field data from Sellafield, UK. *Hydrogeology Journal*, *12*(5), 497–510. https://doi.org/10.1007/s10040-004-0331-7

Molinero, J., Samper, J., & Juanes, R. (2002). Numerical modeling of the transient hydrogeological response produced by tunnel construction in fractured bedrocks. *Engineering Geology*, *64*(4), 369–386. https://doi.org/10.1016/S0013-7952(01)00099-0

Neuman, S. P. (2005). Trends, prospects and challenges in quantifying flow and transport through fractured rocks. *Hydrogeology Journal*, *13*(1), 124–147. https://doi.org/10.1007/s10040-004-0397-2

Noetinger, B. (1994). The Effective Permeability of a Heterogeneous Porous Medium. *Transport in Porous Media*, *15*(2), 99–127. https://doi.org/10.1007/BF00625512

Oda, M. (1985). Permeability tensor for discontinuous rock masses. *Géotechnique*, *35*(4), 483–495. https://doi.org/10.1680/geot.1985.35.4.483

Ouenes, A., & Hartley, L. J. (2000). Integrated fracture reservoir modeling using both discrete and continuum approaches. *Proceedings - SPE Annual Technical Conference and Exhibition*, *PI*, 91–100. https://doi.org/10.2523/62939-ms

Piña, A., Donado, L. D., & Blessent, D. (2019). Analysis of the scale-dependence of the hydraulic conductivity in complex fractured media. *Journal of Hydrology*, *569*(December 2018), 556–572. https://doi.org/10.1016/j.jhydrol.2018.12.006

Priest, S. D. (1993). *Discontinuity Analysis for Rock Engineering* (First). Chapman & Hill. https://doi.org/10.1007/978-94-011-1498-1

Ren, F., Ma, G., Fan, L., Wang, Y., & Zhu, H. (2017). Equivalent discrete fracture networks for modelling fluid flow in highly fractured rock mass. *Engineering Geology*, *229*(July), 21–30. https://doi.org/10.1016/j.enggeo.2017.09.013

Renard, P., & de Marsily, G. (1996). Calculating equivalent permeability: a review. *Advances in Water Resources*, *20*(5–6), 253–278. https://doi.org/10.1016/S0309-1708(96)00050-4

Sævik, P. N., Berre, I., Jakobsen, M., & Lien, M. (2013). A 3D Computational Study of Effective Medium Methods Applied to Fractured Media. *Transport in Porous Media*, *100*(1), 115–142. https://doi.org/10.1007/s11242-013-0208-0

Sanchez-Vila, X., Guadagnini, A., & Carrera, J. (2006). REPRESENTATIVE HYDRAULIC CONDUCTIVITIES IN SATURED GROUNDWATER FLOW. *Reviews of Geophysics*, *44*(3), 1–46. https://doi.org/10.1029/2005RG000169

Scanlon, B. R., Mace, R. E., Barrett, M. E., & Smith, B. (2003). Can we simulate regional groundwater flow in a karst system using equivalent porous media models? Case study, Barton Springs Edwards aquifer, USA. *Journal of Hydrology*, *276*(1–4), 137–158. https://doi.org/10.1016/S0022-1694(03)00064-7

Schulze-Makuch, D., Carlson, D. A., Cherkauer, D. S., & Malik, P. (1999). *Scale Dependency of Hydraulic Conductivity in Heterogeneous Media*. *37*(6), 16. https://doi.org/10.1111/j.1745-6584.1999.tb01190.x

Shah, N., & Ottino, J. M. (1986). Effective transport properties of disordered, multi-phase composites: Application of real-space renormalization group theory. *Chemical Engineering Science*, *41*(2), 283–296. https://doi.org/10.1016/0009-2509(86)87009-9

Siade, A. J., Hall, J., & Karelse, R. N. (2017). A Practical, Robust Methodology for Acquiring New Observation Data Using Computationally Expensive Groundwater Models. *Water Resources Research*, *53*(11), 9860–9882. https://doi.org/10.1002/2017WR020814

Singhal, B. ., & Gupta, R. . (2010). *Applyed Hydrogeology of Fractured Rock* (Second Edi). Springer Science. https://doi.org/10.1007/978-90-481-8799-7

Snow, D. T. (1969). Anisotropic Permeability of Fractured Media. *Water Resources Research*, *5*(6), 1273–1289. https://doi.org/10.1029/WR005i006p01273

Stepanyants, Y. A., & Teodorovich, E. V. (2003). Effective hydraulic conductivity of a randomly heterogeneous porous medium. *Water Resources Research*, *39*(3). https://doi.org/10.1029/2001WR000366

Suescún, L. C. (2016). *Modelación Analítica y numérica para predicción y calibración de caudales de infiltración en obras subterráneas - Túneles* [Universidad Nacional de Colombia]. http://www.bdigital.unal.edu.co/55471/

Teutsch, G. (1993). An extended double-porosity concept as a practical modelling approach for a karstified terrain. *Hydrogeological Processes in Karst Terranes. Proc. International Symposium & Field Seminar, Antalya, Turkey, 1990*, *207*, 281–292.

Tran, T. T.-B. (Stanford U. (1995). *Stochastic simulation of permeability fields and their scale-up for flow modeling*. Stanford University.

Wanfang, Z., Wheater, H. S., & Johnston, P. M. (1997). State of the art of modelling two-phase flow in fractured rock. *Environmental Geology*, *31*(3–4), 157–166. https://doi.org/10.1007/s002540050175

Wang, H. F., & Anderson, M. P. (1982). *Introduction to groundwater modeling: finite difference and finite element methods* (Vol. 66, Issues 1–4). ACADEMIC PRESS, INC. http://books.google.com/books?hl=en&lr=&id=uJT-jwTZQW8C&pgis=1%5Cnhttp://books.google.com/books?hl=en&lr=&id=uJT-jwTZQW8C&oi=fnd&pg=PT4&dq=Introduction+to+Groundwater+Modeling+-+Finite+Difference+and+Finite+Element+Methods&ots=NyKF4rR7_K&sig=kegFjcrHi7Koz

Wang, T., Zhan, S., & Huang, T. (2015). Determining transmissivity of fracture sets with statistical significance using single-borehole hydraulic tests: Methodology and implementation at Heshe well site in central Taiwan. *Engineering Geology*, *198*, 1–15. https://doi.org/10.1016/j.enggeo.2015.09.006

Warren, J. E., & Price, H. S. (1961). Flow in Heterogeneous Porous Media. *Society of Petroleum Engineers Journal*, *1*(03), 153–169. https://doi.org/10.2118/1579-G

Wen, X.-H., & Gómez-Hernandez, J. (1996). Upscaling hydraulic conductivities in

heterogeneous media: An overview. *Journal of Hydrology*, 24. https://doi.org/10.1016/S0022-1694(96)80030-8

Witherspoon, P. A., Wang, J. S. Y., Iwai, K., & Gale, J. E. (1980). Validity of Cubic Law for Fluid Flow in a Deformable Rock Fracture. *Water Resources Research*, *16*(6), 1016–1024. https://doi.org/10.1029/WR016i006p01016

Wyllie, D. C., & Mah, C. W. (2007). Rock Slope Engineering. In *Environmental and Engineering Geoscience* (4th ed., Vol. 13). Taylor & Francis e-Library. https://doi.org/10.2113/gseegeosci.13.4.369

Young, N. L., Reber, J. E., & Simpkins, W. W. (2019). FracKfinder: A MATLAB Toolbox for Computing Three-Dimensional Hydraulic Conductivity Tensors for Fractured Porous Media. *Groundwater*, *57*(1), 75–80. https://doi.org/10.1111/gwat.12837

Zhou, H. (2010). *Three-dimensional hydraulic conductivity upscaling in groundwater modeling* (Vol. 36, Issue 10). UNIVERSIDAD POLITECNICA DE VALENCIA.

Zhou, H., Li, L., & Jaime Gómez-Hernández, J. (2010). Three-dimensional hydraulic conductivity upscaling in groundwater modeling. *Computers and Geosciences*, *36*(10), 1224–1235. https://doi.org/10.1016/j.cageo.2010.03.008

Zhou, Y., & Li, W. (2011). A review of regional groundwater flow modeling. *Geoscience Frontiers*, *2*(2), 205–214. https://doi.org/10.1016/j.gsf.2011.03.003